

Non-Newtonian Slurry Simulant Development and Selection for Pulse Jet Mixer Testing

A. P. Poloski
P. A. Meyer
L. K. Jagoda
P. R. Hrma

August 2004

Prepared for Bechtel National, Inc.
under Contract 24590-101-TSA-W000-0004

LEGAL NOTICE

This report was prepared by Battelle Memorial Institute (Battelle) as an account of sponsored research activities. Neither Client nor Battelle nor any person acting on behalf of either:

MAKES ANY WARRANTY OR REPRESENTATION, EXPRESS OR IMPLIED, with respect to the accuracy, completeness, or usefulness of the information contained in this report, or that the use of any information, apparatus, process, or composition disclosed in this report may not infringe privately owned rights; or

Assumes any liabilities with respect to the use of, or for damages resulting from the use of, any information, apparatus, process, or composition disclosed in this report.

Reference herein to any specific commercial product, process, or service by trade name, trademark, manufacturer, or otherwise, does not necessarily constitute or imply its endorsement, recommendation, or favoring by Battelle. The views and opinions of authors expressed herein do not necessarily state or reflect those of Battelle.



This document was printed on recycled paper.

(9/97)

**Non-Newtonian Slurry Simulant
Development and Selection for
Pulse Jet Mixer Testing**

A. P. Poloski
P. A. Meyer
L. K. Jagoda
P. R. Hrma


for W. Tamosaitis 8/12/04

August 2004

ACCEPTED FOR
PROJECT USE

Test specification: 24590-WTP-TSP-RT-03-008, Rev. 0

Test plan: TP-RPP-WTP-296 Rev 0

Test exceptions: 24590-WTP-TEF-RT-03-060 and
24590-WTP-TEF-RT-03-081

R&T focus area: Pretreatment & Vitrification

Test Scoping Statement(s): B-100

Battelle – Pacific Northwest Division
Richland, Washington 99352

Completeness of Testing

This report describes the results of work and testing specified by Test Specification 24590-WTP-TSP-RT-03-008, Rev. 0 and Test Plan TP-RPP-WTP-296 Rev 0. The work and any associated testing followed the quality assurance requirements outlined in the Test Specification/Plan. The descriptions provided in this test report are an accurate account of both the conduct of the work and the data collected. Test plan results are reported. Also reported are any unusual or anomalous occurrences that are different from expected results. The test results and this report have been reviewed and verified.

Approved:



Gordon H. Beeman, Manager
WTP R&T Support Project



Date

Testing Summary

This document describes work performed by Battelle – Pacific Northwest Division (PNWD) under Test Plan TP-RPP-WTP-296 Rev 0, “Test Plan for Determination of Scaled Performance Data for Pulse Jet Mixers in Prototypic Ultrafiltration Feed Process (UFP) and HLW Lag Storage (LS) Vessels.” Pulse jet mixer (PJM) technology has been selected for mixing non-Newtonian fluids in the Hanford Waste Treatment Plant (WTP).

This report describes the development of nonhazardous, non-Newtonian simulants that were used to evaluate the mixing performance of PJM systems. Both transparent and opaque simulants were developed and used in this testing.

Objectives

This investigation was conducted according to Test Plan TP-RPP-WTP-296 Rev 0 in response to Test Specification 24590-WTP-TSP-RT-03-008 Rev. 0, “Development of Scaled Performance Data for PJM Mixers in the Ultrafiltration Feed and Lag Storage/Blend Tanks.”

The mixing performance in the PJM test vessels needed to be assessed for non-Newtonian fluids. To realize this objective, there was a need to develop non-Newtonian rheological simulants that were non-hazardous and similar in rheological nature to the actual Hanford waste that will be processed in the WTP.

The primary objective of the testing reported in this document was to identify candidate materials and develop recipes for nonhazardous rheological simulants to be used in validation testing of the PJM apparatus. These test objectives were satisfied, as described in Table S.1.

Table S.1. Test Objective Evaluation

Test Objective	Objective Met (Y/N)	Discussion
The objective of this task is to develop simulants that provide data on mobilizing non-Newtonian simulants for the assessment of PJM mixing system designs for UFP and LS vessels.	Yes	This report discusses the development of nonhazardous non-Newtonian rheological simulants that were tested and then used in PJM test vessels for validation testing. A transparent simulant and an opaque simulant were selected for testing in various vessels including UFP and LS scaled prototypes.

Test Exceptions

Table S.2 discusses the test exceptions applied to this test.

Table S.2. Test Exceptions

List Test Exceptions	Describe Test Exceptions
24590-WTP-TEF-RT-03-060	An assessment of PJM mixing performance data is needed to help WTP/DOE ORP make an early decision as to whether an alternative mixing test program needs to be initiated for the WTP non-Newtonian vessels. These PJM performance data were obtained with the use of a transparent simulant, Laponite. Development of the Laponite simulant is described in this report.
24590-WTP-TEF-RT-03-081	Tests are needed to demonstrate adequate mixing in the UFP and LS prototypic configurations deemed to be the best mixing design for the WTP non-Newtonian vessels using a particulate clay simulant that closely matches the rheological properties of actual waste. Development of the particulate clay simulant used for this testing (a mixture of kaolin, bentonite, and water) is described in this report.

Conduct of Testing

Possible raw materials for suitable simulants were identified through literature searches. After evaluation and down selection based on published property data and costs, promising candidates were mixed in small laboratory batches and tested for rheological properties.

Based on the small-scale testing and recipes generated from that testing, three transparent simulants were tested in a single PJM test stand to evaluate the cavern formation and mixing achievable with each of those materials. An optically transparent simulant was selected from these tests, based on its similarity to available real waste data and its properties favorable to scale-up testing. An opaque particulate simulant was also developed and tested in the single PJM test stand.

Results and Performance Against Success Criteria

Ultimately, the scaled testing methodology involved conducting tests in a number of scaled vessels with representative non-Newtonian simulants. To assess the effect of physical scale on mixing performance, five test stands were tested with PJMs; three were used to investigate the scaling laws and two were reduced scaled versions of the full-scale tanks. Scale-up and application of the mixing technologies are based on hydrodynamic theories and developments by the PJM mixing program.

Table S.3 discusses the success criteria provided in Test Specification 24590-WTP-TSP-RT-03-008 Rev. 0, “Development of Scaled Performance Data for PJM Mixers in the Ultrafiltration Feed and LAG Storage/Blend Tanks.”

Table S.3. Discussion of Test Success Criteria

List Success Criteria	Explain How the Tests Did or Did Not Meet the Success Criteria
Tests will be deemed successful if non-Newtonian simulants that match the critical parameters required for validation testing can be developed and used.	Simulants from four materials were developed and tested successfully in a single PJM test stand. Two simulants, one opaque and one transparent, were selected for continued testing of prototypic systems.
Scaled testing with the same simulant(s) in both the 336 Building tank (4 PJMs) and the APEL scaled tank (4 PJMs) will be able to demonstrate that the nondimensional results are the same or close enough at different scales.	Simulants developed had the right rheological properties and were resilient enough to be tested in both test stands and compared on a rheological basis at critical points of testing to help determine the nondimensional scaling results.

Acronyms

BNI	Bechtel National Inc.
GFC	glass forming chemical
HLW	high-level waste
LAW	low-activity waste
M&TE	measuring and test equipment
NIST	National Institute of Standards and Technology
PJM	pulse jet mixer
PNWD	Battelle – Pacific Northwest Division
PSD	particle size distribution
QA	Quality Assurance
QAPjP	Quality Assurance Project Plan
RPP	River Protection Project
R&T	Research and Technology
UDS	undissolved solids
VSL	Vitreous State Laboratory
WTP	Waste Treatment Plant
WTPSP	Waste Treatment Plant Support Project

Contents

Testing Summary	iii
Acronyms	vii
1.0 Introduction	1.1
2.0 Quality Requirements	2.1
3.0 Rheological Considerations.....	3.1
3.1 Rheological Background.....	3.1
3.1.1 Flow Curves.....	3.1
3.1.2 Shear Strength and Yield Stress.....	3.5
3.1.3 Deborah Number.....	3.9
3.2 WTP Process Stream Rheology	3.11
3.2.1 Flow Curves.....	3.11
3.2.2 Shear Strength.....	3.12
4.0 Pulse Jet Mixer Technology Considerations	4.1
4.1 Cavern Formation with Steady Jets	4.2
4.2 Cavern Formation with Unsteady Jets	4.4
5.0 PJM Simulant Objectives	5.1
5.1 Transparent Simulant Objectives	5.2
5.2 Opaque Simulant Objectives.....	5.2
6.0 Simulant Selection.....	6.1
6.1 Transparent Simulant Evaluation.....	6.7
6.2 Transparent Simulant Development	6.7
6.2.1 Laponite Recipe	6.8
6.2.2 Carbopol Recipe	6.10
6.2.3 Xanthan Gum Recipe.....	6.13
6.2.4 Transparent Simulant PJM Testing.....	6.15
6.2.5 Transparent Simulant PJM Testing Downselect.....	6.18
6.3 Opaque Simulant Evaluation	6.21
6.4 Opaque Simulant Development	6.22
7.0 Conclusions	7.1
8.0 References	8.1

Figures

1.1	RPP-WTP Basic Process Flowsheet	1.2
1.2	Example of Mixing Behavior with PJM Technology	1.3
3.1	Diagram of Fluid Flow Between Stationary and Moving Plates	3.1
3.2	Rheograms of Various Fluid Types	3.3
3.3	Rheogram Illustrating the Concept of Dynamic and Static Yield Stress	3.6
3.4	Geometrical Requirements of a Shear Vane	3.7
3.5	Typical Response of a Shear Vane	3.8
3.6	Schematic of Cone and Plate Sensor System Used to Measure Normal Force Behavior	3.9
3.7	Rheograms of Laboratory-Scale HLW Pretreated Sludge Samples.....	3.12
3.8	Shear Strength as a Function of Gel Time for HLW Pretreated Sludge	3.13
3.9	Ratio of Shear Strength to Yield Stress as a Function of Gel Time for HLW Pretreated Sludge...	3.14
4.1	Diagram of Significant Variables in PJM Vessels.....	4.1
6.1	Micrographs of Laponite Particles	6.8
6.2	Laponite RD Shear Strength as a Function of Concentration in Hanford Process Water.....	6.9
6.3	Laponite Shear Strength as a Function of Temperature and Gel Time.....	6.9
6.4	Micrographs of Carbopol Particles	6.10
6.5	Shear Strength Response of Carbopol Ultraez-10 at Various Concentrations	6.11
6.6	Correlation Between Bingham Yield Stress and Carbopol Concentration	6.11
6.7	Correlation Between Bingham Consistency and Carbopol Concentration	6.12
6.8	Correlation Between Casson Yield Stress and Carbopol Concentration	6.12
6.9	Chemical Structure of Xanthan Gum.....	6.13
6.10	Correlation Between Shear Strength and Xanthan Gum Concentration	6.14
6.11	Correlation Between Bingham Yield Stress and Xanthan Gum Concentration	6.14
6.12	Correlation Between Bingham Consistency and Xanthan Gum Concentration	6.15
6.13	Flow Curves of Laponite Samples Drawn from PJM Mixing Caverns	6.16
6.14	Flow Curves of Carbopol Samples Drawn from PJM Mixing Caverns.....	6.17
6.15	Flow Curves of Xanthan Gum Samples Drawn from PJM Mixing Caverns	6.17
6.16	Comparison of Transparent Simulant Flow Curves to the WTP HLW Pretreated Sludge Upper Rheological Bound at Ambient Temperature	6.19
6.17	Nondimensional PJM Scaling Correlation for Several Simulants and Operating Conditions	6.19
6.18	Deborah Number as a Function of Flow Distance in a PJM Vessel	6.21
6.19	Correlation Between Bingham Consistency and Kaolin-Bentonite Concentration	6.23
6.20	Correlation Between Bingham Yield Stress and Kaolin-Bentonite Concentration	6.23
6.21	Shear Strength as a Function of Gel Time for Kaolin-Bentonite Simulant at Various Solids Concentrations at Ambient Temperature	6.24
6.22	Kaolin-Bentonite Shear Strength as a Function of Temperature and Gel Time	6.24

Tables

3.1 Typical Shear Rates Observed in Several Common Processing Applications.....	3.2
3.2 Viscosities of Several Common Newtonian Fluids	3.3
3.3 Bingham Plastic Model Fit to Several Food Items	3.4
3.4 Shear Strength of Some Common Foods.....	3.8
3.5 Rheological Parameters for Various Viscoelastic Fluids at 25°C.....	3.10
3.6 Physical and Rheological Properties for HLW Pretreated Sludge.....	3.11
5.1 Significant Simulant Properties for PJM Performance and Goal Values.....	5.1
5.2 Significant Transparent Simulant Properties for PJM Performance and Goal Values.....	5.2
5.3 Significant Opaque Simulant Properties for PJM Performance and Goal Values	5.3
6.1 Summary of Literature Search Results for Potential Simulants.....	6.2
6.2 Scoring Table of Potential Transparent Simulants.....	6.7
6.3 Significant Opaque Simulant Properties for PJM Performance and Goal Values	6.18
6.4 Scoring Table of Potential Opaque Simulants	6.21
7.1 Summary of Significant Transparent Simulant Properties for PJM Performance	7.1
7.2 Summary of Significant Opaque Simulant Properties for PJM Performance and Goal Values	7.2

1.0 Introduction

The Hanford Site has 177 single- and double-shell tanks containing radioactive waste. The U.S. Department of Energy (DOE) Office of River Protection's Waste Treatment Plant (WTP) is being designed and built to pretreat and then vitrify a large portion of these wastes. The WTP consists of three primary facilities: a pretreatment facility, a low-activity waste (LAW) vitrification facility, and a high-level waste (HLW) vitrification facility. The pretreatment facility receives waste feed from the Hanford tank farms and separates it into 1) a high-volume, low-activity, liquid process stream stripped of most solids and radioisotopes and 2) a much smaller-volume HLW slurry containing most of the solids and most of the radioactivity. In the pretreatment facility, solids and radioisotopes are removed from the waste by precipitation, filtration, and ion exchange processes to produce the LAW streams. The slurry of filtered solids is blended with two ion exchange eluate streams containing soluble radioisotopes to produce the HLW stream. The HLW and LAW vitrification facilities convert these process streams into glass, which is poured directly into stainless steel canisters. The major unit operations of the WTP are shown on the process flowsheet presented in Figure 1.1.

The process stream significant to this report is identified on the diagram as "HLW pretreated sludge." Several vessels through which the HLW pretreated sludge stream will be processed will be mixed using pulse jet mixer (PJM) technology. This technology has been selected for use in so called "black cell" regions of the WTP. Within these regions of the plant, maintenance capability will not be available for the operating life of the WTP. PJM technology was selected for use in these regions because of the lack of moving mechanical parts that require maintenance.

The concept behind PJM technology involves a pulse tube coupled with a jet nozzle. One end of the tube is immersed in the tank, while periodic vacuum, vent, and pressurized air are supplied to the opposite end. Application of vacuum, vent, and pressurized air creates various operating modes for the pulse tube, including the drive cycle (pressure), where the contents of the PJM tube are discharged at high velocity through the nozzle; the refill mode (vacuum), where the tank contents refill the pulse tube; and an equilibration mode (vent), where the pulse tube and tank fill levels approach the same level. The PJM system uses these operating modes to produce a sequence of drive cycles that form a turbulent mixing cavern at the bottom of the tank (see Figure 1.2). PJM operating parameters, velocity, nozzle diameter, and drive time, along with the rheological properties of the fluid being mixed, all contribute to the effectiveness of mixing within the tank.

The volume of this mixing cavern as a function of PJM operating parameters and rheological properties is significant in evaluating the performance of the PJM system. Consequently, an effort was undertaken to investigate PJM performance in scaled versions of PJM vessels with simulants whose rheological behavior is similar to that of the actual pretreated HLW sludge. Simulants were used because the actual waste is chemically hazardous and highly radioactive. The simulant selected for testing had to minimize cost and schedule impacts. Thousands of gallons of simulant were required for the tests, and the simulant needed to be nonhazardous to minimize workplace risk and disposal issues.

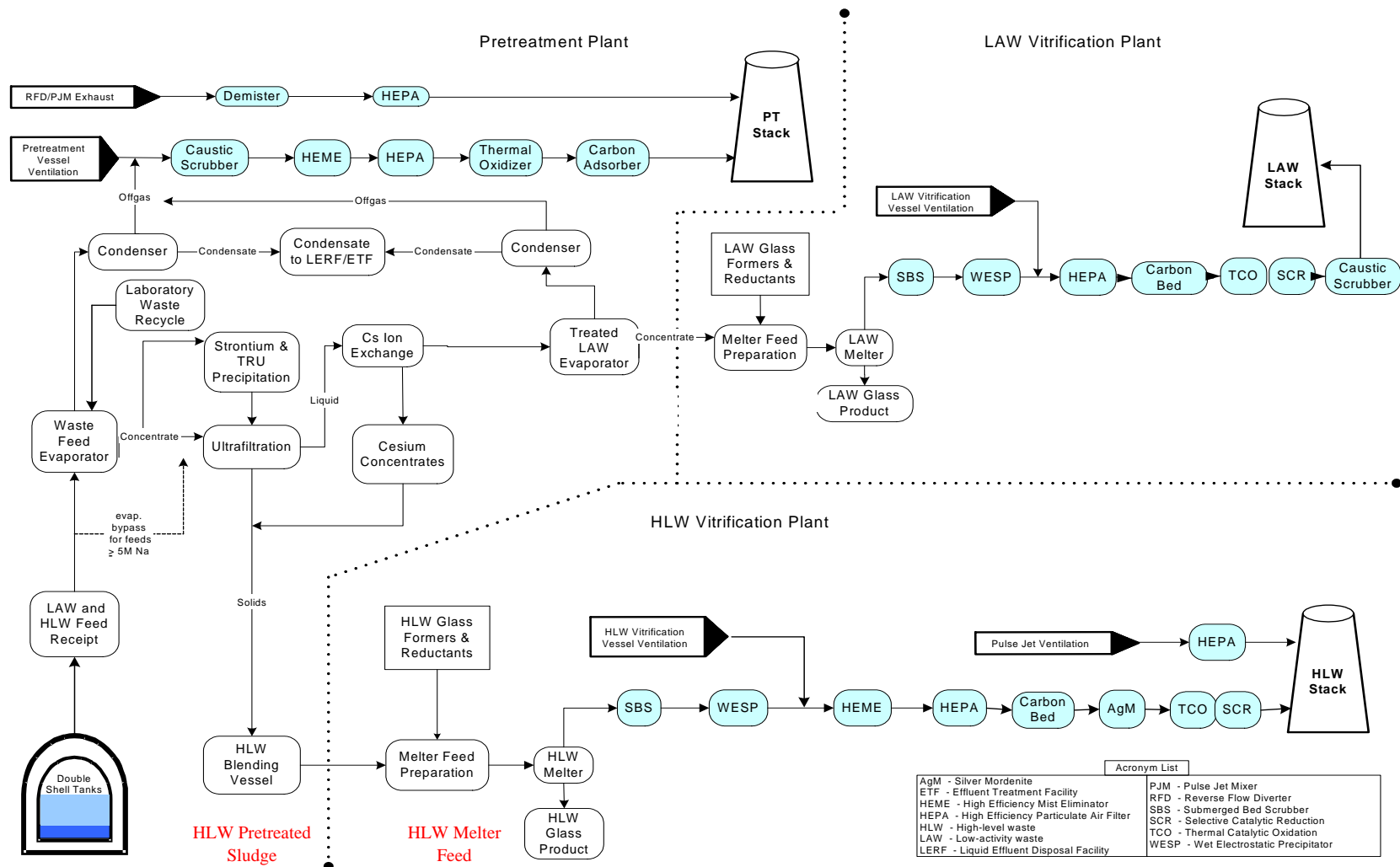


Figure 1.1. RPP-WTP Basic Process Flowsheet

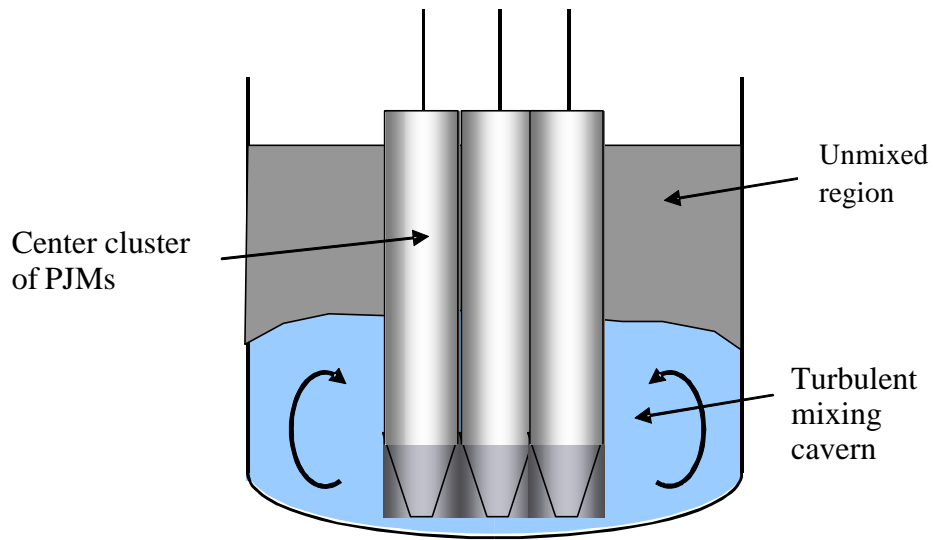


Figure 1.2. Example of Mixing Behavior with PJM Technology

The simulant development strategy consisted of conducting a literature search to find materials that could be manipulated to match target upper bounding rheological conditions established by Bechtel National, Inc. (BNI). Cost, schedule, safety, and disposal needs for large scale testing in the PJM test stands were considered in the selection process.

After materials were identified, laboratory-scale development testing was done to further down select and refine recipes. Four simulants were tested in the single PJM test stand to study cavern formation. These tests led to the selection of two simulants, one transparent and one opaque, that were used for further PJM testing. This report describes in detail the development of the simulants selected for this PJM performance evaluation effort.

2.0 Quality Requirements

PNWD implemented the RPP-WTP quality requirements by performing work in accordance with the PNWD Waste Treatment Plant Support Project quality assurance project plan (QAPjP) approved by the RPP-WTP Quality Assurance (QA) organization. This work was performed to the quality requirements of NQA-1-1989 Part I, Basic and Supplementary Requirements, and NQA-2a-1990, Part 2.7. These quality requirements were implemented through PNWD's *Waste Treatment Plant Support Project (WTPSP) Quality Assurance Requirements and Description Manual*. The analytical requirements were implemented through WTPSP's Statement of Work (WTPSP-SOW-005) with the Radiochemical Processing Laboratory (RPL) Analytical Service Operations (ASO).

Experiments that were not method-specific were performed in accordance with PNWD's procedures QA-RPP-WTP-1101, "Scientific Investigations," and QA-RPP-WTP-1201, "Calibration Control System," ensuring that sufficient data were taken with properly calibrated measuring and test equipment (M&TE) to obtain quality results.

As specified in Test Specification 24590-WTP-TSP-RT-03-008 Rev. 0, "Development of Scaled Performance Data for PJM Mixers in the Ultrafiltration Feed and Lag Storage/Blend Tanks," BNI's QAPjP, PL-24590-QA00001, was not applicable because the work was not performed in support of environmental/regulatory testing, and the data will not be used as such.

PNWD addressed internal verification and validation activities by conducting an Independent Technical Review of the final data report in accordance with PNWD's procedure QA-RPP-WTP-604. This review verified that the reported results were traceable, that inferences and conclusions were soundly based, and the reported work satisfied the Test Plan objectives. This review procedure is part of PNWD's *WTPSP Quality Assurance Requirements and Description Manual*.

3.0 Rheological Considerations

The first step in developing a rheological simulant was to understand the important properties of the actual material that needed to be simulated. This section presents an overview of important rheological concepts followed by a summary of actual HLW pretreated sludge rheological measurements. A set of upper bounding rheological properties is also presented. These bounding properties represent the target rheological values to which the simulants were designed.

3.1 Rheological Background

3.1.1 Flow Curves

Rheology is defined as the study of the flow of matter (Steffe 1996). When a force (i.e., stress) is placed on a fluid, the fluid deforms or strains. Many relationships have been defined that relate stress to strain for various fluids. Flow behavior of a fluid can generally be explained by considering a fluid of thickness x placed between two solid plates (see Figure 3.1). The lower plate is held stationary while a force F is applied to the upper plate of area A and results in the plate moving at velocity v . If the plate moves at length ΔL , the strain, γ , on the fluid can be defined by Eq. (3.1).

$$\gamma = \frac{\Delta L}{x} \quad (3.1)$$

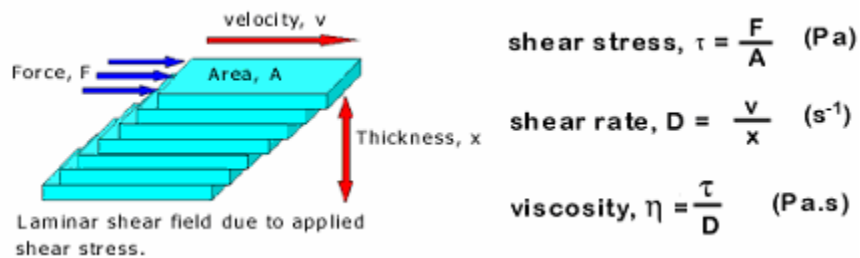


Figure 3.1. Diagram of Fluid Flow Between Stationary and Moving Plates (Plates Not Shown in Figure)

The rate of change of strain (also called shear rate), $\dot{\gamma}$, can be defined by Eq. (3.2). Because the shear rate is defined as the ratio of a velocity to a length, the units of the variable are the inverse of time, typically s^{-1} :

$$\dot{\gamma} = \frac{d\gamma}{dt} = \frac{d}{dt} \left(\frac{\Delta L}{x} \right) = \frac{v}{x} \quad (3.2)$$

Typical shear rates observed in several common processing operations can be seen in Table 3.1. Depending on the application, shear rates in the range of 10^{-6} to $10^7 s^{-1}$ are possible.

Table 3.1. Typical Shear Rates Observed in Several Common Processing Applications (Steffe 1996)

Situation	Shear Rate Range (1/s)	Typical Applications
Sedimentation of Particles in a Suspending Liquid	$10^{-6} - 10^{-3}$	Medicines, paints, spices in salad dressing
Leveling due to surface tension	$10^{-2} - 10^{-1}$	Frosting, paints, printing inks
Draining under gravity	$10^{-1} - 10^1$	Vats, small food containers
Extrusion	$10^0 - 10^3$	Snack and pet foods, toothpaste, cereals, pasta, polymers
Calendaring	$10^1 - 10^2$	Dough sheeting
Pouring from a Bottle	$10^1 - 10^2$	Foods, cosmetics, toiletries
Chewing and Swallowing	$10^1 - 10^2$	Foods
Dip Coating	$10^1 - 10^2$	Paints, confectionery
Mixing and Stirring	$10^1 - 10^3$	Food processing
Pipe Flow	$10^0 - 10^3$	Food processing, blood flow
Rubbing	$10^2 - 10^4$	Topical application of creams and lotions
Brushing	$10^3 - 10^4$	Brush painting, lipstick, nail polish
Spraying	$10^3 - 10^5$	Spray drying, spray painting, fuel atomization
High speed coating	$10^4 - 10^6$	Paper
Lubrication	$10^3 - 10^7$	Bearings, gasoline engines

The shear stress applied to the fluid can be found from Eq. (3.3). Because the shear stress is defined as the ratio of a force to an area, the units of the variable are pressures, typically Pa (N/m^2):

$$\tau = \frac{F}{A} \quad (3.3)$$

The apparent viscosity of the fluid is defined as the ratio of the shear stress to shear rate (Eq. 3.4). Because the viscosity is defined as the ratio of shear stress to shear rate, the units of the variable are Pa•s. Typically, viscosity is reported in units of centipoise (cP) where $1 \text{ cP} = 1 \text{ mPa}\cdot\text{s}$:

$$\eta(\dot{\gamma}) = \frac{\tau(\dot{\gamma})}{\dot{\gamma}} \quad (3.4)$$

For Newtonian fluids, the apparent viscosity is independent of shear rate (see Eq. 3.5). Examples of the viscosity of common Newtonian materials can be seen in Table 3.2.

Table 3.2. Viscosities of Several Common Newtonian Fluids (Steffe 1996)

Material	Viscosity at 20°C (mPa•s)
Acetone	0.32
Water	1.0
Ethanol	1.2
Mercury	1.6
Ethylene Glycol	20
Corn Oil	71
Glycerin	1,500

$$\tau = \eta \dot{\gamma} \quad (3.5)$$

where τ is the shear stress, η is the Newtonian viscosity, and $\dot{\gamma}$ is the shear rate.

Fluids that do not behave as Newtonian fluids are referred to as non-Newtonian. Rheograms, or plots of shear stress versus shear rate, are typically used to characterize non-Newtonian fluids. Examples of typical rheograms can be seen in Figure 3.2.

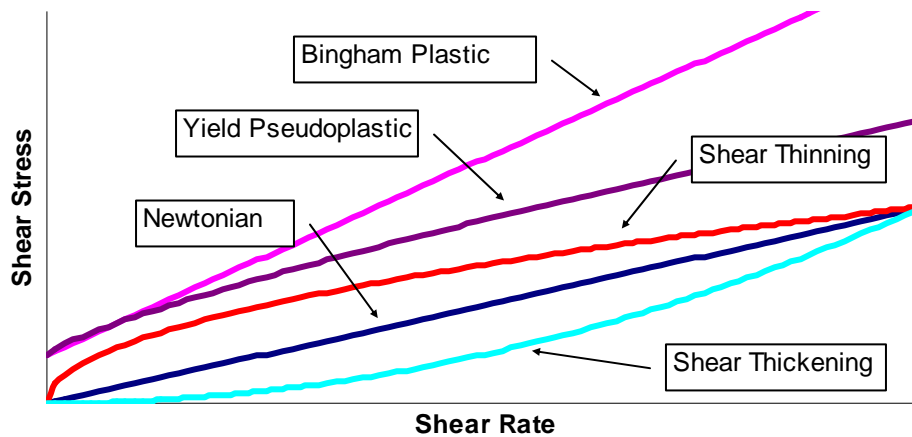


Figure 3.2. Rheograms of Various Fluid Types

Shear-thinning and shear-thickening fluids can be modeled by the Ostwald equation (3.6). If $n < 1$, the material is referred to as pseudoplastic (shear thinning). If $n > 1$, that material is referred to as dilatant (shear thickening). These fluids exhibit decreasing or increasing apparent viscosities as shear rate increases, depending on whether the fluid is shear thinning or shear thickening, respectively. Because shear-thickening flow behavior is rare, it is often an indication of possible secondary flow patterns or other measurement errors:

$$\tau = m\dot{\gamma}^n \quad (3.6)$$

where m is the power-law consistency coefficient, n is the power-law exponent, and $\dot{\gamma}$ is the shear rate.

When a rheogram has a non-zero y-intercept, that fluid is said to possess a yield stress. A yield stress is a shear-stress threshold that defines the boundary between solid-like and fluid-like behavior. The fluid will not begin to flow until the yield stress threshold is exceeded. Therefore, yield pseudoplastic and Bingham plastic rheograms do not pass through the origin. Yield pseudoplastic rheograms are often fit with Herschel-Bulkley or Casson equations.

For Bingham plastic materials, once enough force has been applied to exceed the yield stress, the material approaches Newtonian behavior at high shear rates (Eq. 3.7). Because Bingham plastic behavior is used throughout this document, a Bingham plastic model was fit to rheological data for several common food items (Table 3.3). Many of these items would not typically be classified as Bingham plastic materials. The purpose of the Bingham plastic model fits is to provide the reader with a relative understanding of the magnitude of Bingham plastic values used in this document compared with common materials. Human perception is typically based on a shear rate of approximately 60 s^{-1} . This shear rate roughly compares to stirring a fluid with a kitchen utensil or pouring a fluid from a bottle.

$$\tau = \tau_y + k\dot{\gamma} \quad (3.7)$$

where τ_y is the Bingham yield stress, k is the Bingham consistency, and $\dot{\gamma}$ is the shear rate.

Table 3.3. Bingham Plastic Model Fit to Several Food Items (Steffe 1996)

Material	Consistency (cP)	Yield Stress (Pa)	R ²
Squeeze Margarine	49	11	0.80
Ketchup	190	38	0.81
Whipped Desert Topping	190	45	0.80
Tub Margarine	320	125	0.77
Mustard	400	50	0.84
Mayonnaise	610	130	0.80
Whipped Butter	660	350	0.75
Stick Butter	690	240	0.77
Stick Margarine	860	350	0.77
Whipped Cream Cheese	910	480	0.75
Peanut Butter	1,200	570	0.75
Apple Butter	1,600	300	0.82
Canned Frosting	1,900	450	0.79
Honey	15,000	5.3	1.00
Marshmallow Cream	23,000	1,200	0.92

Fluids that exhibit a nonlinear rheogram with yield stress are modeled by the three-parameter Herschel-Bulkley equation (3.8). Again, shear-thickening behavior is uncommon, and typically the Herschel-Bulkley power-law exponent is less than unity:

$$\tau = \tau_{H,0} + k_H \dot{\gamma} \quad (3.8)$$

where

- $\tau_{H,0}$ = yield stress
- k_H = Herschel-Bulkley consistency coefficient
- b = Herschel-Bulkley power law exponent
- $\dot{\gamma}$ = shear rate.

A similar equation for nonlinear rheograms with a yield point is the two-parameter Casson equation (3.9). This equation is used to model various materials, including melted chocolate:

$$\tau = \left((\tau_{C,0})^{0.5} + k_C \dot{\gamma}^{0.5} \right)^2 \quad (3.9)$$

where

- $\tau_{C,0}$ = yield stress
- k_C = Herschel-Bulkley consistency coefficient
- $\dot{\gamma}$ = shear rate.

The rheological parameters discussed above may be a function of the previous shear history placed on the fluid. This is referred to as thixotropy or rheopexy and appears as a time-dependent response to shear. When subjected to a fixed shear rate, thixotropic fluids decrease in viscosity over time, while rheopectic fluids increase with viscosity over time. Often thixotropy is seen as a large initial viscosity loss followed by gradual further loss. Once shear is removed, thixotropic fluids may recover their viscosity, not instantaneously, but over a period of time. Thixotropy is much more common than rheopexy; therefore, only thixotropy will be considered further in this report.

3.1.2 Shear Strength and Yield Stress

Steffe (1996) explains that many methods have been developed to evaluate yield stress. These methods produce varying results based on the rheological technique and assumptions used in the evaluation. To explain these variations, the concept of static and dynamic yield stress is introduced. The idea behind static and dynamic yield stress can be explained by assuming that there are two structures that present yield stress-exhibiting fluids. One structure is insensitive to shear rate and defines the dynamic yield stress associated with a flow curve. However, a second, weak structure is also present that forms while the fluid is at rest. This structure is sensitive to shear rate and breaks down as the fluid is sheared. Combined, these two stresses define the static yield stress value (Figure 3.3).

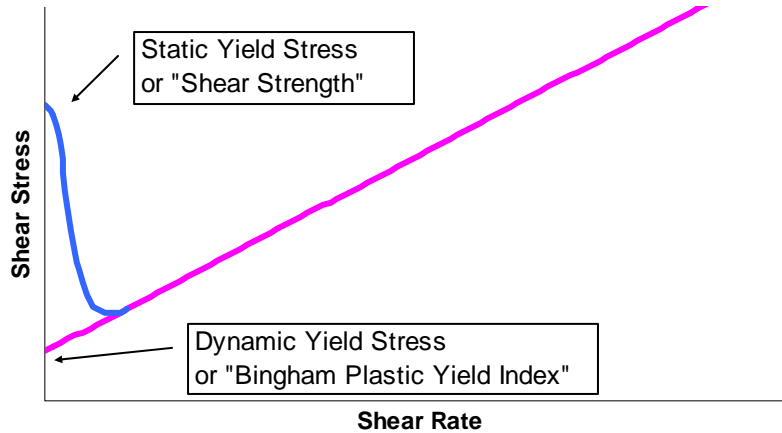


Figure 3.3. Rheogram Illustrating the Concept of Dynamic and Static Yield Stress

The use of static and dynamic yield stress values varies with application. For instance, the dynamic yield stress value extrapolated from a rheogram should be used when performing laminar pipeline head-loss calculations. The static yield stress should be used for process restart applications where the second structure could form while the fluid is at rest. In general, there is no established relationship between the two parameters. Because static yield stress is a cumulative function, the value is always greater than or equal to the dynamic value.

A common method of measuring the static shear strength of a fluid is with a device called a shear vane. A WTP procedure for measuring the static yield stress of a fluid was provided by Smith and Prindiville (2002). The WTP adopted convention is to refer to the static yield stress as “shear strength.” The dynamic yield stress is often referred to as yield stress or yield index.

The shear vane measurement technique involves slowly rotating a vane immersed in the sample material and measuring the resulting torque as a function of time. The torque can be converted to shear stress by making several assumptions (Liddell and Boger 1996). First, the material is assumed to be sheared only along the cylinder defined by the dimensions of the vane. This assumption has been shown to be only a slight oversimplification. The actual diameter of the sheared surface may be up to 5% larger than the vane dimensions (Bowles 1977; Keentok 1982; Keentok et al. 1985). Second, it is assumed that the stress is distributed uniformly over the cylindrical sheared surface. Although the stress actually peaks sharply at the vane peaks (Barnes and Carnali 1985; Keentok et al. 1985), it has been shown that the error due to this assumption is minimal (Alderman et al. 1991; Avramidis and Turain 1991; James et al. 1987; Nguyen and Boger 1983, 1985a, 1985b). Therefore, a good approximation of the measured stress can be calculated from Eq. (3.10), where K is the vane constant defined in Eq. (3.11):

$$\tau_s = T / K \quad (3.10)$$

$$K = \frac{\pi D^3}{2} \left(\frac{H}{D} + \frac{1}{3} \right) \quad (3.11)$$

where

- τ_s = calculated shear stress (Pa)
- T = measured torque (Nm)
- K = shear vane constant (m^3)
- D = shear vane diameter (m)
- H = shear vane height (m).

In addition, the shear vane must be immersed in the test material such that wall and end effects are negligible. Figure 3.4 shows an accepted material testing geometry to minimize wall and end effects (Dzuy and Boger 1985). These geometry requirements were confirmed prior to material testing.

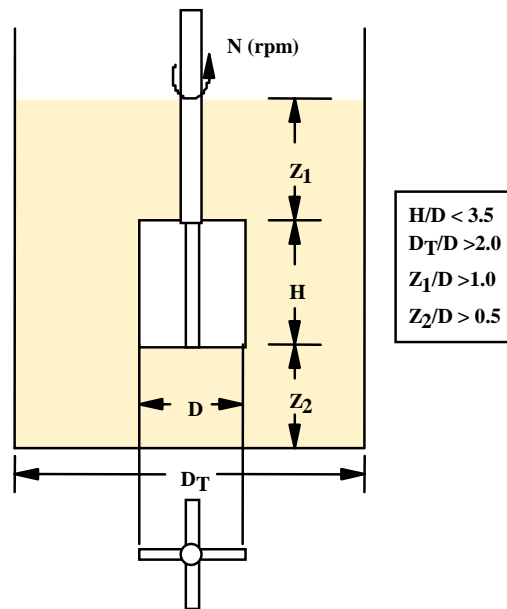


Figure 3.4. Geometrical Requirements of a Shear Vane

A typical stress-time profile is shown in Figure 3.5. The profile shows an initial linear region followed by a nonlinear region, a stress maximum, and a stress decay region. The shape of the stress time profile can be explained from a consideration of the network bonds within the material. The initial linear region represents the elastic deformation of the network bonds. The nonlinear region represents viscoelastic flow (also called creep flow), where the network bonds are stretched beyond their elastic limit and some of the bonds begin to break. At the maximum stress point on the curve, the majority of the bonds are broken and the material begins to flow as a fully viscous fluid. The network typically collapses, and stress decay is observed. This peak on the curve is defined as the shear strength, and it indicates the minimum force required to cause material deformation or flow.

From this response two shear strengths can be defined: one corresponding to the transition between elastic and viscoelastic flow and the other corresponding to the transition between viscoelastic and fully viscous flow, τ_s . Most researchers regard the transition between viscoelastic and fully viscous flow as the definitive shear strength of the material. In this report, shear strength is defined by the transition between viscoelastic and fully viscous flow, τ_s .

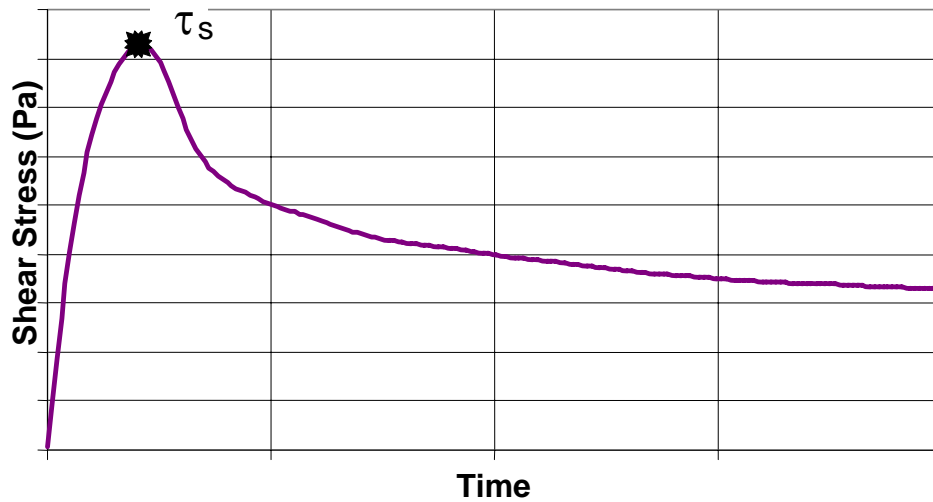


Figure 3.5. Typical Response of a Shear Vane

Because shear strength values are discussed throughout this document, values of shear strength for some common food items as measured by the vane method are given in Table 3.4. This table provides a reference point based on human perception of common foods for the magnitude of shear strength values discussed later in this document.

Table 3.4. Shear Strength of Some Common Foods (Steffe 1996)

Material	Shear Strength (Pa)
Baby food, peaches	22.9 ± 3.4
Spaghetti sauce, Brand B	24.8 ± 3.4
Spaghetti sauce, Brand A	26.3 ± 4.5
Tomato puree, Brand B	30.0 ± 4.2
Baby food, pears	31.8 ± 5.0
Tomato puree, Brand A	34.4 ± 3.7
Tomato ketchup, Brand B	43.2 ± 3.4
Apple sauce, Brand B	48.2 ± 4.7
Tomato ketchup, Brand A	51.3 ± 5.0
Baby food, carrots	64.0 ± 4.0
Apple sauce, Brand A	77.3 ± 0.0
Mustard, Brand A	82.5 ± 5.3
Mustard, Brand B	103.8 ± 5.0
Mayonnaise, Brand B	163.8 ± 4.2
Mayonnaise, Brand A	204.4 ± 5.0

3.1.3 Deborah Number

As explained by McBain et al. (2000), the Deborah number quantifies the difference between the deformation behavior of (elastic) solids and (viscous) liquids. In an elementary explanation following Lapasin and Pricl (1995), the Deborah number, De , is defined as the ratio between a characteristic relaxation time, t_r , of the material and a characteristic residence time of the deformation process under observation, t_p :

$$De = \frac{t_r}{t_p} \quad (3.12)$$

The relaxation time is zero for an inelastic viscous fluid and infinite for an elastic solid. The rheological properties of a substance can be easily classified as liquid-like when the relaxation time is much shorter than the residence time and as solid-like when it is much longer. In other words, high Deborah numbers correspond to solid-like behavior and low Deborah numbers to liquid-like behavior. In the intermediate region, materials may display a combination of both properties, and their behavior is called viscoelastic. Material relaxation times range from picoseconds for water or atmospheric air and nanoseconds for mineral oils through microseconds to kiloseconds for various polymer solutions and melts to megaseconds for glass (Tanner 1988).

As discussed in Section 3.1.1, when a Newtonian fluid is placed between two flat parallel plates that are moved laterally with respect to each other, a resisting frictional force is developed proportional to the area of the plate, the relative velocity of the plates (divided by the gap) and the viscosity of the fluid. However, when a non-Newtonian viscoelastic fluid such as a polymer solution or melt is placed between the plates, an additional force normal to the plates is also exerted. A common way to determine normal force behavior experimentally is with cone and plate rheometer systems, as shown in Figure 3.6.

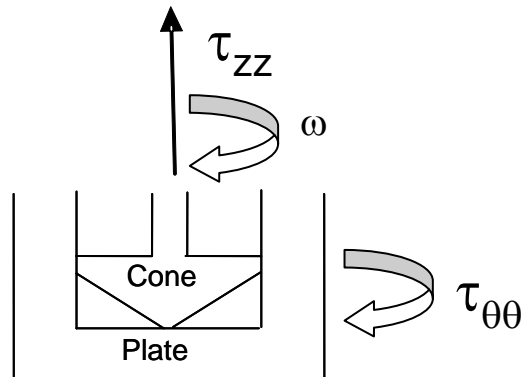


Figure 3.6. Schematic of Cone and Plate Sensor System Used to Measure Normal Force Behavior

Each non-Newtonian material is unique and so is each process. Because the relaxation time for many non-Newtonian fluids is a function of the shear rate, t_r depends on the process conditions. Conversely, process conditions generally vary with time and position; hence, t_p also varies with process conditions.

For a viscoelastic fluid subjected to a steady shear flow, the relaxation time is given by the formula (Chhabra and Richardson 1999):

$$t_r = \frac{N_1}{2\tau\dot{\gamma}} \quad (3.13)$$

where N_1 is the first normal stress difference, τ is the shear stress parallel to flow, and $\dot{\gamma}$ is the shear rate. The first normal stress difference is defined as $N_1 = \tau_{zz} - \tau_{\theta\theta}$, where τ_{zz} is the normal stress in the direction of flow and $\tau_{\theta\theta}$ is the normal stress in the direction perpendicular to flow. In this situation, t_r is a function of the shear rate, because N_1 and τ also depend on the shear rate. Typical experimental data allow for a power law approximation of N_1 and τ (see Eq. 3.7) as functions of the shear rate:

$$N_1 = m_1(\dot{\gamma})^{n_1} \quad (3.14)$$

The equation becomes

$$t_r = m_r(\dot{\gamma})^{n_r} \quad (3.15)$$

where $m_r = m_1/(2m)$ and $n_r = n_1 - n - 1$. Because n_1 does not typically exceed unity, n_r is negative (Table 3.5) (Solomon et al. 1981). Therefore, at small shear rates (i.e., $\dot{\gamma} \rightarrow 0$) the relaxation time approaches infinity and decreases toward zero as the shear rate approaches infinity. Physically this indicates that viscoelastic fluids behave as solids at low shear and high process times. Conversely, viscoelastic fluids behave as liquids at high shear and high process times.

Table 3.5. Rheological Parameters for Various Viscoelastic Fluids at 25°C (Solomon et al. 1981)

Material	m (N s ⁻ⁿ m ⁻²)	n	m_1 (N s ^{-n₁} m ⁻²)	n_1	m_r (s ^{-n_r})	n_r
4.5 wt% Xanthan Gum	50.0	0.13	6.73	0.46	0.067	-0.67
1.4 wt% CMC	16.6	0.41	6.37	0.52	0.19	-0.89
0.30 wt% Carbopol (pH 4.4)	31.9	0.24	1.54	0.61	0.024	-0.63
2.0 wt% Xanthan Gum	20.0	0.16	2.13	0.57	0.053	-0.59
0.8 wt% CMC	4.11	0.53	2.33	0.57	0.28	-0.96
0.17 wt% Carbopol (pH 4.4)	11.2	0.29	0.218	0.84	0.0097	-0.45

3.2 WTP Process Stream Rheology

3.2.1 Flow Curves

As part of the design effort for the WTP, samples of actual Hanford tank waste were taken and processed through laboratory-scale unit operations similar to the flowsheet shown in Figure 1.1. At various stages of laboratory-scale processing, the samples were characterized for multiple properties, including several rheological and physical properties. The physical and rheological properties from several of these tanks processed to the HLW pretreated sludge stage were compiled in a recent WTP report (Poloski 2004). The rheological properties are listed in Table 3.6. These data indicate that the HLW pretreated sludge can be characterized by a Bingham plastic rheological model. As the solids loadings in these samples increase, the corresponding rheological parameters increase significantly. Poloski et al. (2003) explain that recent published research on slurry rheology indicates that the rheological properties increase asymptotically as the solids loading increases toward the maximum achievable packing for a given sample type. The HLW pretreated sludge can be described as washed and leached with the interstitial liquid composed primarily of 0.01 M NaOH solution and trace amounts of dissolved solids. Therefore, when water content is measured to calculate the weight percent total solids, the contribution due to the dissolved solids is considered negligible, and the value can be considered the weight percent of undissolved solids (UDS).

Table 3.6. Physical and Rheological Properties for HLW Pretreated Sludge (Poloski 2004)

Description (proposed bounding conditions)	Total Solids (wt%)	Slurry Density (g/mL)	Consistency (cP)	Yield Stress (Pa)
Pretreated HLW Sludge AZ-101	10	1.08	<10	0
Pretreated HLW Sludge AZ-101	15	1.12	5.2	2.9
Pretreated HLW Sludge AZ-101	22	1.19	10.5	11.4
Pretreated HLW Sludge AZ-102	15	1.14	30	18.5
Pretreated HLW Sludge AZ-102	20	1.17	34	26.3
Pretreated HLW Sludge AZ-102	25	1.24	99	209.1
Pretreated HLW Sludge C-104	5	1.0	3	0.2
Pretreated HLW Sludge C-104	15	1.05	5	0.4
Pretreated HLW Sludge C-104	25	1.12	10	5.8

This study also compared the rheological measurements with the unit operations to be performed in the WTP to propose a set of bounding rheological and physical properties. The recommended upper bounding conditions are to limit the Bingham plastic rheological properties to 30 cP for Bingham consistency and 30 Pa for Bingham yield stress. This proposed upper bound is shown along with actual rheograms in Figure 3.7. The AZ-102 20 wt% Bingham and Power Law curve fits are also shown in this figure.

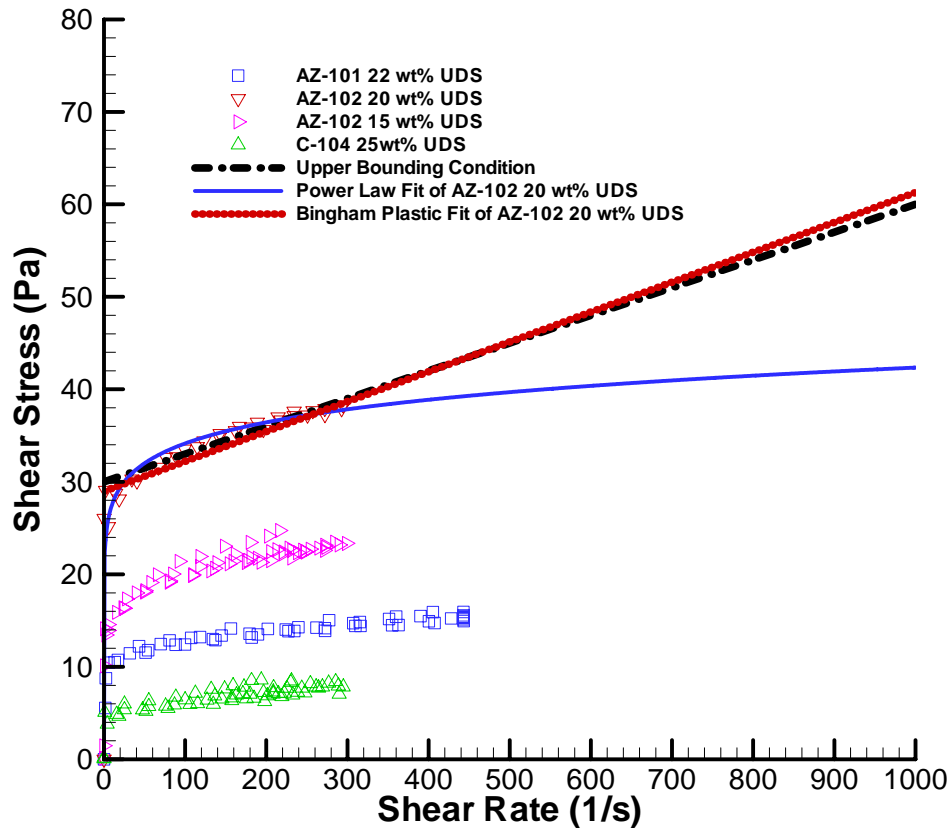


Figure 3.7. Rheograms of Laboratory-Scale HLW Pretreated Sludge Samples

Each of the HLW pretreated waste rheograms shown in Figure 3.7 fits well with the Bingham plastic, Ostwald, or Herschel-Bulkley rheological models. However, the actual measurements were limited to relatively low shear rates due to instrumentation limitations. Actual waste processing involves shear rates that exceed this range. By using the definition of apparent viscosity defined by Eq. (3.4) with each of the rheological models defined by Eq. (3.6) for Ostwald, (3.7) for Bingham plastic, and (3.8) for Herschel-Bulkley, an equation for apparent viscosity as a function of shear rate for each rheological model can be derived. Taking the limit of apparent viscosity as shear rate approach infinity reveals that the Ostwald and Herschel-Bulkley equations trend toward zero apparent viscosity, while the apparent viscosity of the Bingham plastic tends toward the consistency value. Consequently, the Ostwald and Herschel-Bulkley equations likely underpredict flow resistance when extrapolating to higher shear rates. Due to the increased shear thinning of the HLW pretreated sludge (i.e., the curvature shown in the rheograms), the Bingham plastic model provides a conservative bound when extrapolating to higher shear rates. On this basis, the Bingham plastic model was selected over the Ostwald and Herschel-Bulkley equations for characterizing WTP process streams.

3.2.2 Shear Strength

Poloski et al. (2003) also recommended a bound of 625 Pa for shear strength based on restart of mechanical agitators and pipeline plugging calculations. Unfortunately, shear strength was not measured historically on the HLW pretreated sludge samples. However, one set of shear strength measurements

was obtained during characterization of AZ-101 HLW pretreated sludge (Poloski 2004). A 22-wt% UDS pretreated HLW sludge sample was agitated (stirred) and allowed to sit undisturbed for various periods of time (referred to as gel time) between measurements. This methodology allowed investigation into how the shear strength of sludge rebuilds after being sheared. Results are shown in Figure 3.8.

Speers et al. (1987) described this rebuild behavior for several drilling mud slurries with a first-order rate model (Eq. 3.16). This model appears to be a good fit to the shear strength data shown in Figure 3.8. The best fit parameters for this model are shown below. Using this model, the initial shear strength parameter (16.8 Pa) should agree roughly with the measured rheological Bingham yield stress measurement (11.4 Pa). By taking the ratio of the shear strength to the yield stress, the y-axis of Figure 3.8 is nondimensionalized, and the resulting plot is shown in Figure 3.9. This plot indicates that the shear strength rebuilt immediately from the time that it remained unshered. A steady-state shear-strength-to-yield-stress ratio of approximately 2.7 was established after approximately 18 hours of gel time. The steady-state condition was defined by a threshold point where the model predicted 99% of the steady-state growth:

$$\tau_s = A(1 - e^{-Bt}) + C \quad (3.16)$$

where

τ_s = shear strength (Pa)	See Figure 3.8 ($r^2=0.929$)
t = gel time (hour)	0 to 120 hours
A = initial ($t = 0$ hour) shear strength (Pa)	16.8 Pa
B = time constant (hour^{-1})	0.262 hr^{-1}
C = difference between initial and steady state shear strength (Pa)	14.2 Pa.

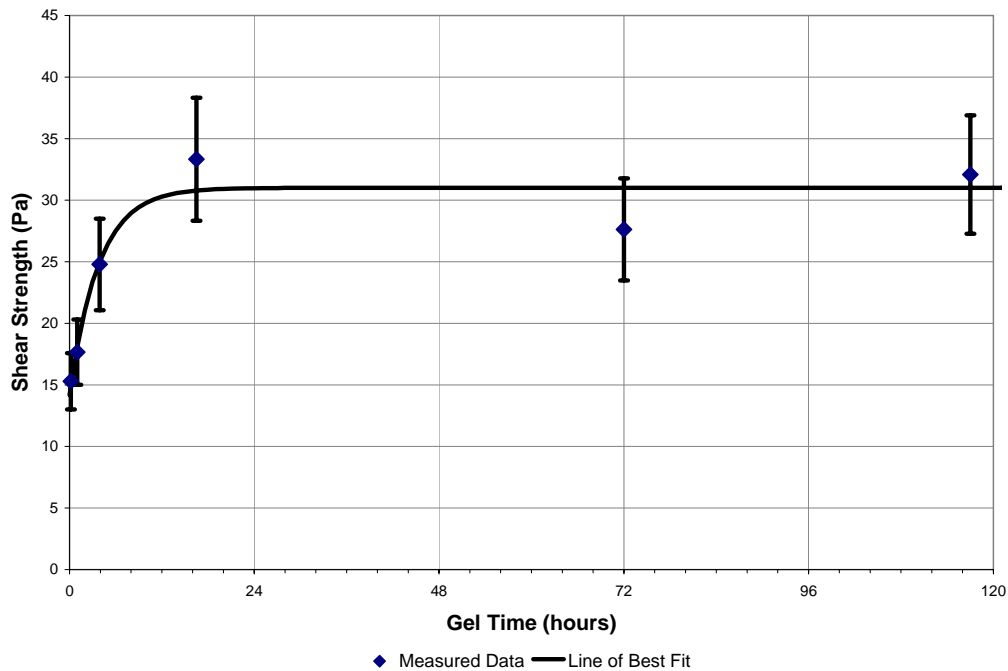


Figure 3.8. Shear Strength as a Function of Gel Time for HLW Pretreated Sludge (Poloski et al. 2003)

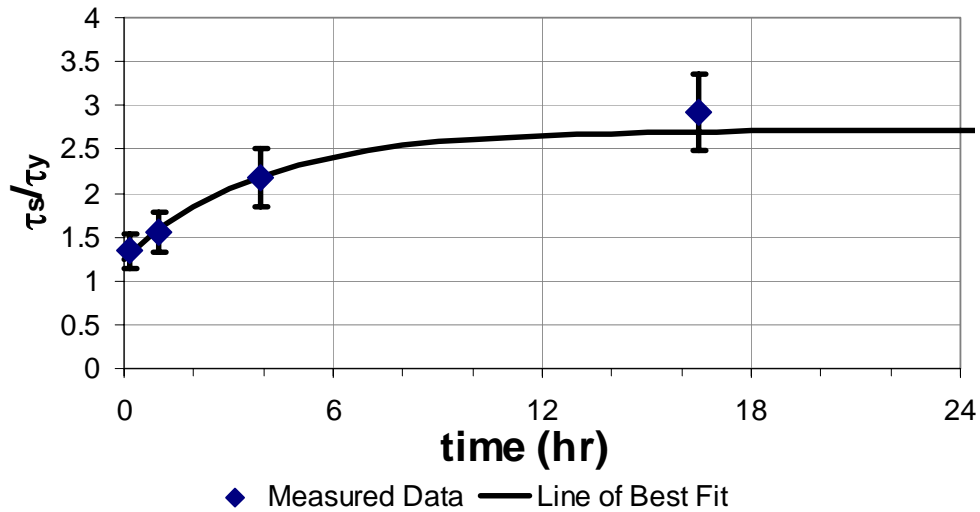


Figure 3.9. Ratio of Shear Strength to Yield Stress as a Function of Gel Time for HLW Pretreated Sludge

Shear strength is a function of packing efficiency of the solid particles, particle shape, particle size distribution, density of the solids particles, pH, viscosity of suspending medium, ionic strength of suspending medium, and density of suspending medium. Therefore, one expects the shear strength behavior of a particular slurry to be similar to that of a slurry with similar particles and suspending medium. Given the absence of shear strength data for other HLW pretreated sludges, the HLW pretreated sludge was assumed to consist of similar solid particles and suspending medium. Accordingly, the shear strength of an HLW pretreated sludge sample was estimated by measuring the yield stress of the sample and using the nondimensional correlation shown in Figure 3.9. Applying this concept to the hypothetical bounding condition HLW sample with a yield stress of 30 Pa estimated a steady-state shear strength of approximately $2.7 \times 30 \text{ Pa} = 80 \text{ Pa}$. The 80-Pa shear strength value was an extrapolated single data point for HLW pretreated sludge based on best engineering judgment. Actual shear strength values for other HLW pretreated sludge from other waste tanks may exceed the 80 Pa value discussed above.

4.0 Pulse Jet Mixer Technology Considerations

A schematic of a typical PJM system is shown in Figure 4.1. In this figure, the tank has diameter D_T , volume V_T , and operating level H . There are N PJM tubes in the tank, each with diameter D_{PT} and volume V_{PT} . Each PJM has a conical nozzle with diameter d_0 . For baseline WTP designs, the total volume of the pulse tubes, $N \cdot V_{PT}$, is approximately 10% of the operating volume of the vessel.

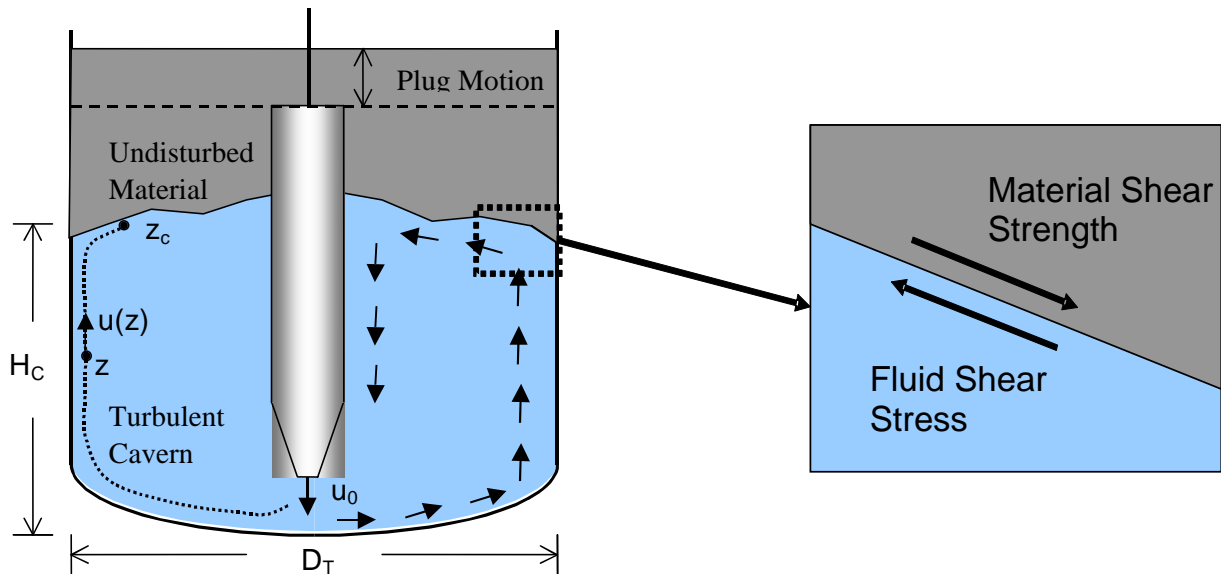


Figure 4.1. Diagram of Significant Variables in PJM Vessels

A mixing cavern in a PJM system forms because the fluid motion created by the jet decreases with distance away from the jet nozzle. At some point, fluid velocities are low enough that resulting fluid stresses are no longer able to overcome the shear strength of the non-Newtonian material. Hence, a force balance occurs that is stable (illustrated in Figure 4.1). As the jet velocity increases, fluid velocity increases and the cavern grows. As the strength of the non-Newtonian material increases, the cavern becomes smaller. A successful mixing system design places agitators so there are no regions of stationary material in the mixing vessel.

Cavern formation is highly dependent on the rheological properties of the slurry. As discussed in Section 3.2, rheological tests with HLW pretreated sludge samples suggest that the waste can be represented by the Bingham plastic rheological model. While this laminar flow behavior information is useful, it does not describe adequately all the relevant rheology for the cavern formation problem. For instance, before it is disturbed, the actual waste slurry is quiescent and develops shear strength, τ_s , as a function of gel time (see Section 3.2).

Additionally, turbulent conditions exist inside the cavern. This implies that a wide range of large shear forces and shear rates are present in the cavern at any given moment. As discussed in Section 3.2, at large shear rates the flow behavior is approximated by the Bingham consistency. Additional corrections for fluid flow behavior are necessary for turbulent flow regimes, and rheological data on the

turbulent flow of HLW pretreated sludge are not available. As velocity slows at the interface, it will at some point re-laminarize. Under these conditions the laminar Bingham rheology will apply directly. As shear rates decrease toward zero, the Bingham yield stress may be an important parameter in the boundary layer at the cavern interface. It is generally believed that this boundary layer region is quite thin and the effects of yield stress are minor. However, the topic of turbulent to laminar transition in a non-Newtonian slurry is not well understood, and it is possible that yield stress in the boundary layer affects the position of the cavern.

4.1 Cavern Formation with Steady Jets

In this section, we present a simple theory for the position of the cavern for a single steady turbulent jet. Figure 4.1 illustrates a single PJM system in a vessel with a non-Newtonian slurry. The discharging jet impinged on the tank bottom, then moved up the side wall and turned inward. It is assumed that the flow inside the cavern is fully turbulent and approximately Newtonian. Three-dimensional Newtonian turbulent jets, whether free (away from boundaries) or impinging on boundaries, are known to follow the law (Rajaratnam 1976):

$$u(z) = c_J \frac{u_0 d_0}{z} \quad (4.1)$$

In Eq. (4.1), z is the distance to any point along the primary path the jet travels, $u(z)$ is the maximum time averaged velocity at point z , and c_J is a constant that takes into account the effects of geometry. The value of c_J for common Newtonian jets generally ranges between 1 and 6. It is assumed that Eq. (4.1) is approximately true for a turbulent, non-Newtonian particulate slurry.

If the cavern is well established (steady state), a force balance exists at the cavern interface. The stress exerted by the turbulent flow at the cavern equals the shear strength of the undisturbed slurry. The cavern interface is assumed to be a solid surface with a turbulent boundary layer.^(a) The turbulent fluid shear stress at some point along the interface z_c can be expressed as

$$\tau_f = C_f \frac{1}{2} \rho u_c^2 \quad (4.2)$$

where u_c is the average maximum velocity at point z_c , and C_f is a wall frictional coefficient. In both laminar and turbulent flow boundary layers, wall friction coefficients typically depend on the viscous Reynolds number^(b) according to

$$C_f = c_R Re^{-1/b} \quad (4.3)$$

(a) A boundary layer is normally thought of as the region of decreasing velocity at a solid surface created by a free stream away from the wall. For a turbulent wall jet, there is little distinction between the jet and the boundary layer because the peak mean flow velocity is often very near the wall. Boundary layer refers loosely to the turbulent flow at the cavern interface.

(b) The wall friction coefficient may also depend on the Bingham yield stress to some degree due to laminar flow in the viscous sublayer of the turbulent boundary layer. This effect is hypothesized to be small and is as yet unproven.

where c_R and b are constants and Re is the viscous Reynolds number defined by

$$Re = \frac{\rho U \delta}{\mu} \quad (4.4)$$

Here U is the local velocity, δ is the local length scale (typically the thickness of the boundary layer or the distance along the boundary layer to the point of interest), and μ is the viscosity. The viscosity used in evaluating the Reynolds number is the consistency k from the Bingham plastic rheological model.

If Eq. (4.4) is evaluated at point z_c ($U = u_c$ and $\delta = z_c$), then Eq. (4.1) can be written $Re = c_J Re_0$, where Re_0 is the jet Reynolds number given by

$$Re_0 = \frac{\rho u_0 d_0}{\mu} \quad (4.5)$$

Hence Eq. (4.3) can be written

$$C_f = c_J c_R Re_0^{-1/b} \quad (4.6)$$

The exponent parameter b is typically about 4–5 for many turbulent boundary layers. Hence the friction coefficient is not a strong function of jet Reynolds number. The wall shear stress given by Eq. (4.2) is therefore primarily determined by the jet velocity with only a minor correction for viscous Reynolds number.

Continuing with the derivation, a force balance at the cavern interface is written by setting $\tau_f = \tau_s$, so Eq. (4.2) becomes

$$C_f \frac{1}{2} \rho u_c^2 = \tau_s \quad (4.7)$$

If the distance of cavern growth from the PJM nozzle, z_c , is approximated as the distance from the center of the tank to the tank wall plus the distance up the tank wall to the mixing cavern,

$$z_c \approx H_c + \frac{D_T}{2} \quad (4.8)$$

Then from Eq. (4.1), (4.7), and (4.8) an expression for the position of the cavern can be written:

$$H_c = c_J u_0 d_0 \sqrt{\frac{\rho C_f}{2\tau_s} - \frac{D_T}{2}} \quad (4.9)$$

If the yield Reynolds number, Re_τ , is introduced,

$$Re_\tau = \frac{\rho u_0^2}{\tau_s} \quad (4.10)$$

Then Eq. (4.9) combined with (4.6) and (4.10) gives

$$\frac{H_c}{D_T} = a \frac{d_0}{D_T} Re^{-1/2b} Re_\tau^{1/2} - \frac{1}{2} \quad (4.11)$$

where a is a constant. Because Eq. (4.11) is such a weak function of viscous Reynolds number,^(a) a simplified expression for the cavern height may be written as

$$\frac{H_c}{D_T} = a \frac{d_0}{D_T} Re_\tau^{1/2} - \frac{1}{2} \quad (4.12)$$

where it is understood that the constant coefficients a in Eq. (4.11) and (4.12) are different.

Eq. (4.11) is generalized to account for all potential Reynolds number effects as well as bottom curvature effects by writing

$$\frac{H_c}{D_T} = c_1 \frac{d_0}{D_T} f(Re) Re_\tau^{1/2} - c_2 \quad (4.13)$$

Eq. (4.13) is the most general form of an expression for cavern height. Experiments at different Reynolds numbers (geometric scales) are required to determine the constants, c_1 , and c_2 , as well as the functional form of $f(Re)$.

4.2 Cavern Formation with Unsteady Jets

The results presented in the previous section were for a steady turbulent jet. In this section the effects of pulsation on the position of the cavern are examined. There are several potential effects associated with the periodic, non-steady discharge of the PJMs. These may be hydrodynamic or rheological.

The primary hydrodynamic issue is that of establishing flow. Any real jet has a finite time required to establish steady flow conditions. If the jet is turned off before this, the velocity far from the jet will be less than that of the steady jet. The time for a steady jet to be fully established, t_{ss} , can be estimated by considering the time it takes a fluid element to travel from the jet to the cavern. By recognizing that $u(z) = dz/dt$, and using boundary conditions of at $t = 0$, then $z = 0$; and at $t = t_{ss}$, then $z = z_c$. Eq. (4.1) can be integrated to obtain

(a) When $b \approx 5$, the exponent on Re is approximately -0.1.

$$t_{ss} = \frac{\left(H_c + \frac{D_r}{2}\right)^2}{2c_J u_0 d_0} \quad (4.14)$$

From Eq. (4.14) it is seen that the flow establishment time increases with the square of the cavern height and is reduced by increasing jet velocity or nozzle size. The flow establishment time can be examined by writing H_c in terms of its dependent parameters. Combining Eq. (4.14) with (4.9) and (4.10) gives

$$t_{ss} = \frac{c_J C_f}{4} \text{Re}_\tau \frac{d_0}{u_0} \quad (4.15)$$

The volumetric flow of material out of the PJM nozzle is given by $Q = u_0 \cdot (\pi/4) \cdot d_0^2$, while the same volumetric flow rate calculated from the volume discharged over the drive time is given as $Q = (\pi/4) \cdot d_{PT}^2 \cdot \Delta L / t_D$. The PJM drive time is then determined as follows:

$$t_D = \frac{V_p}{\frac{\pi}{4} d_0^2 u_0} \quad (4.16)$$

where $V_p = (\pi/4) \cdot d_{PT}^2 \cdot \Delta L$ is the volume of a pulse. The ratio of drive time to flow establishment time is therefore

$$\frac{t_D}{t_{ss}} = \frac{16V_p}{\pi c_J C_f d_0^3 \text{Re}_\tau} \quad (4.17)$$

From Eq. (4.17) the ratio of drive time to flow establishment is seen to depend only on the pulse volume, the nozzle diameter, and the yield Reynolds number.

To obtain an expression for the cavern height for the case of a pulse jet, we need to understand how the velocity at the cavern changes as a function of time. Assuming that the spatial and time dependence of the jet are independent,

$$u(z, t) = u_{ss}(z) f(t) \quad (4.18)$$

where u_{ss} is given by Eq. (4.1) and $f(t)$ must be determined. To estimate the function $f(t)$, it is assumed that the rate of change of the velocity at any point z is proportional to the difference between the velocity and the steady-state value, with the constant of proportionality equal to the time for flow establishment, t_{ss} :

$$\frac{du(z,t)}{dt} = \frac{u_{ss}(z) - u(z,t)}{t_{ss}} \quad (4.19)$$

Substituting Eq. (4.18) into (4.19), one can separate variables and integrate using the boundary condition of $f(0) = 0$. Using this boundary condition assumes that flow is stopped at the beginning of the drive cycle:

$$f(t) = 1 - e^{-\frac{t}{t_{ss}}} \quad (4.20)$$

Substituting (4.20) and (4.1) into (4.18) at $t = t_D$ yields

$$u(x, t_D) = \frac{c_j u_0 d_0}{z} (1 - e^{-t_D/t_{ss}}) \quad (4.21)$$

As expected, Eq. (4.21) shows that in the limit of very short drive times the velocity goes to zero. When the drive time is large compared with the flow establishment time, the steady jet solution is recovered.

To obtain an expression for the cavern height with an unsteady jet, the analysis of the previous section is repeated, using Eq. (4.21) instead of (4.1). The resulting expression is

$$\frac{H_c}{D_T} = c_1 \frac{d_0}{D_T} f(\text{Re}) \text{Re}_\tau^{1/2} (1 - e^{-t_D/t_{ss}}) - c_2 \quad (4.22)$$

Substituting Eq. (4.17) into (4.22) and generalizing the constants results in

$$\frac{H_c}{D_T} = c_1 \frac{d_0}{D_T} f(\text{Re}) \text{Re}_\tau^{1/2} (1 - e^{-C_3 \frac{V_p}{d_0^3 \text{Re}_\tau}}) - c_2 \quad (4.23)$$

The results show that a pulse jet's ability to erode a cavern diminishes significantly if the relative pulse time is short. As the velocity is increased, the relative pulse time diminishes with the square of the velocity according to Eq. (4.16). Subsequently, there is insufficient time to establish the steady flow velocity at the cavern, and a reduced cavern height results. It is clear from examining Eq. (4.23) that a limiting cavern height exists for a given system.

5.0 PJM Simulant Objectives

From the mathematical model of PJM performance described in Section 4, several rheological parameters were identified that are significant to the performance of a PJM mixing vessel. Eq. (4.23) showed that the mixing cavern height is a weak function of Bingham Reynolds number (Re) and a strong function of yield Reynolds number (Re_y), which is a function of density and shear strength. In the case of a non-Newtonian fluid that has been recently agitated (e.g., loaded into the PJM vessel for mixing), the yield Reynolds number can be calculated with the Bingham yield stress rather than the shear strength of the fluid. The Bingham Reynolds number is a function of density and Bingham consistency. Though the density affects both the Bingham and yield Reynolds numbers, it is not as important as the other three parameters. This is because density likely varies only over the range of 1.0 to 1.25 g/mL, while the other parameters are likely vary over several decades.

Therefore, for this simulant development effort, our objective was to develop a simulant that matched these parameters with the HLW pretreated sludge values. These significant rheological parameters and HLW pretreated sludge values (see Section 3.2) are shown in Table 5.1.

Table 5.1. Significant Simulant Properties for PJM Performance and Goal Values

Property	Goal Values
Density	1.2 g/mL
Bingham Consistency	30 cP
Bingham Yield Stress	30 Pa
Shear Strength	80 Pa

Because the performance equations are nondimensional, PJM performance testing was done at various scales. Additionally, changes in rheological behavior were considered, and a perfect match to the properties listed in Table 5.1 was deemed desirable but not necessary. A two-stage testing strategy was implemented to develop a recommended PJM design for the WTP. The first stage was to test a four-pulse-tube PJM system at large and small scale and compare the results to confirm the scaled testing approach. The tests were performed with the same simulant and with the PJM system operated the same way in both vessels. Cavern heights were measured as a function of PJM operation parameters and compared nondimensionally so that a scaling law could be determined.

With a scaling law confirmed, a second round of testing took place. In this second stage, a set of potential WTP PJM vessel configurations was tested at small scale in scaled prototypic vessels. The mixing performance of these configurations was determined and a single configuration selected as a recommended design.

The existence of a scaling law was then used to relate the results in scaled prototypic vessels to planned full-scale plant conditions. This was done by comparing PJM performance at identical nondimensional operating conditions. Because no length scale exists in the yield Reynolds number, the shear strength of the simulant had to match the shear strength of the actual waste for this nondimensional parameter to match at the same PJM jet velocity.

If the material has been loaded into the PJM vessel recently, its yield stress can be used to compute the yield Reynolds number. In this case, the yield stress of the simulant should also match the yield stress of the actual waste for the yield Reynolds number to match at the same PJM jet velocity.

However, the Bingham Reynolds number (a secondary nondimensional parameter) does possess a length scale. For this nondimensional parameter to match at the same PJM jet velocity, a small-scale simulant should possess a smaller consistency value. The full-scale consistency of 30 cP was specified as a simulant goal, making this a conservative small-scale simulant.

5.1 Transparent Simulant Objectives

To evaluate the performance of the PJM system, the cavern height was measured under various operating and rheological conditions. Rather than use complex instrumentation and techniques to determine the cavern height with an opaque simulant, a set of transparent simulants was developed to allow the cavern height to be measured visually. If constrained to transparent simulants, however, it is unlikely that all of the goals for the properties listed in Table 5.1 could be achieved. Thus the most significant property of the scaling law, shear strength, was selected as a primary design variable.

The transparent simulant was the primary simulant for the first stage of testing. Development of the scaling law required testing different operating conditions and shear strengths. In a scenario where the HLW pretreated sludge in the WTP remained quiescent for several hours and then the PJM system was restarted, the target shear strength was approximately 80 Pa (see Section 3.2). In another scenario where HLW pretreated sludge was loaded into an operating PJM vessel, the shear strength of the sludge did not grow above the yield stress of the material, and the yield stress value, 30 Pa, was used in the yield Reynolds number. Therefore, the shear strength of the simulant was also adjustable from roughly 10 to 100 Pa (Table 5.2).

Table 5.2. Significant Transparent Simulant Properties for PJM Performance and Goal Values

Property	Goal Values	Potential Testing Range
Shear Strength	<ul style="list-style-type: none"> • 30 Pa (normal operation) • 80 Pa (restart condition) 	10–100 Pa

5.2 Opaque Simulant Objectives

For the second stage of the testing strategy for scaled prototypes, an additional simulant was developed. This second simulant was designed to account for the properties listed in Table 5.1 that are not listed in Table 5.2. Because of the limited number of tests performed, opaque simulants were used. Tracer techniques and sensor probes were used to measure mixing cavern size. Discussion of these techniques, however, is outside the scope of this report.

This simulant was used to test normal operation of the PJM system. During normal operation the HLW pretreated sludge was initially sheared and not allowed to remain quiescent and to gel. In this

scenario, the shear strength of the sludge did not grow above the yield stress of the material, and the yield stress value, 30 Pa, was used in the yield Reynolds number. Therefore, the yield stress of the material was the primary design parameter. Testing at different yield Reynolds numbers was accomplished by varying the yield stress, which was adjustable between roughly 10 and 50 Pa. The consistency and density varied due to the adjustment of the yield stress, but they were relatively close to the actual waste bounding values and range of measured rheological properties discussed in Section 3.2 (Table 5.3).

Table 5.3. Significant Opaque Simulant Properties for PJM Performance and Goal Values

Property	Goal Values	Potential Testing Range
Density	1.2 g/mL	1.1–1.2 g/mL
Bingham Consistency	30 cP	10–50 cP
Bingham Yield Stress	30 Pa	10–50 Pa

6.0 Simulant Selection

Development of a simulant for use in the PJM systems involved consideration of many issues, including the following:

- **Safety** – Because testing took place in relatively large amounts, 100 to 10,000 gallons, the simulants needed to be nonhazardous. Loading, unloading, and sampling of the simulant presented many opportunities for personnel to be exposed, and working in personal protective equipment for several hours during a test would have added undesirable complications to the PJM testing.
- **Shear Strength** – As discussed in Section 5, this was a primary control variable for the first stage of testing with the transparent simulants. The simulant had to be able to achieve the range of values listed in Table 5.2.
- **Transparency** – During the first stage of testing, a transparent simulant was used so that cavern height could be measured visually (see Section 5). The simulant had to be transparent enough that a determination of motion could be made several feet into the simulant.
- **Yield Stress** – As discussed in Section 5, this was a primary control variable for the second stage of testing using the opaque simulants. The simulant had to be able to achieve the range of values listed in Table 5.3.
- **Consistency** – As discussed in Section 5, this was a secondary control variable for the second stage of testing using the opaque simulants. The simulant had to be able to achieve the range of values listed in Table 5.3.
- **Thixotropy** – Cavern formation in a PJM vessel took several hours to reach steady state. During this time, the simulant was exposed to shear forces. If the simulant was thixotropic, the Bingham yield stress and consistency varied during the test and may have affected the cavern height in an unknown manner. If a simulant developed shear strength, the material was considered thixotropic, and a trade-off existed between thixotropy and the shear strength of the simulant. The ideal transparent simulant possessed a shear strength that, once exceeded, would instantaneously exhibit constant rheological parameters. Therefore, it was desirable for the material to develop constant flow behavior quickly during the test and to have little thixotropic behavior.
- **Easy of preparation/disposal** – Because testing occurred at scales from 100 to 10,000 gallons, sample preparation techniques/equipment varied. Initially, simulant recipes were developed at laboratory scale in beakers. For the small-scale tests, simulants were prepared in 55-gallon drums with drum mixers. For the large-scale tests, sample preparation was subcontracted to a chemical manufacturer. When scaling a recipe up from laboratory to bench scale and then to production scale, complex preparation procedures often led to large deviations from target simulant properties. In addition, the waste disposal process needed to be short to limit accumulation of spent simulant during testing.
- **Expense** – For the large-scale tests, 10,000 gallons of simulant were procured. To minimize the impact of this quantity on the WTP project, the cost of the simulant had to be considered.

- **Stability** – Testing took place over several weeks, during which the simulant needed to have constant rheological properties. During each test, the simulant was exposed to shear forces that could have degraded the simulant and changed its rheological properties. Over several days of testing, aging (e.g., hydration), and biological growth (e.g., bacteria and algae) might have changed rheological properties; that possibility needed to be considered.

A literature search revealed two classes of fluids that appeared to meet these requirements. For transparent simulants, rheological modifiers for the food and cosmetic industry appeared to be a good choice. For opaque simulants, drilling fluids and various mineral slurries were a good choice. A summary of general information for several rheological modifiers used in the food and cosmetic industry is shown in Table 6.1 (Braun and Rosen 1999; Ciullo 1996; Davidson 1980; van Olphen 1977).

Table 6.1. Summary of Literature Search Results for Potential Simulants

Material	Characteristics
Clay Minerals	<p><i>Description:</i> clay platelets that swell with water and form a flocculated network</p> <p><i>Transparency:</i> transparent (Laponite); opaque (bentonite; kaolinite)</p> <p><i>Rheology:</i> thixotropic; shear thinning with yield stress</p> <p><i>Cost:</i> inexpensive</p> <p><i>Stability:</i> unaffected by shear, temperature, microorganisms, enzymes or UV light</p>
Xanthan Gum	<p><i>Description:</i> soluble anionic polysaccharide</p> <p><i>Transparency:</i> translucent (some grades transparent)</p> <p><i>Rheology:</i> excellent yield stress; very shear thinning at low concentrations ~<5%</p> <p><i>Cost:</i> inexpensive</p> <p><i>Stability:</i> fairly high resistance to shear, temperature, microorganisms, enzymes,</p>

Table 6.1. Summary of Literature Search Results for Potential Simulants

Material	Characteristics
Carbomers	<p>UV light</p> <p><i>Description:</i> anionic carboxyvinyl polymers made by chemically cross-linking poly acrylic acid; water soluble, producing acidic solutions that must be neutralized; often referred to by the trade name Carbopol®</p> <p><i>Transparency:</i> transparent</p> <p><i>Rheology:</i> shear thinning, possesses excellent yield value</p> <p><i>Cost:</i> inexpensive</p> <p><i>Stability:</i> generally resistant to shear, heat, bacterial/enzyme degradation, and UV light</p>
Polyacrylates	<p><i>Description:</i> anionic polymers produced by emulsion polymerization of acrylic acid; often sold as thin emulsions of poly acrylic acid that give clear solutions when neutralized</p> <p><i>Transparency:</i> transparent</p> <p><i>Rheology:</i> sodium polyacrylate is shear thinning with some yield stress; many variations are available, giving almost any desired rheology</p> <p><i>Cost:</i> variable</p> <p><i>Stability:</i> susceptible to shear degradation</p>
Tragacanth	<i>Description:</i> comes from

Table 6.1. Summary of Literature Search Results for Potential Simulants

Material	Characteristics
Gum	<p>bushes that grow in the mountains of countries from Pakistan to Greece, particularly Iran and Turkey</p> <p><i>Transparency:</i> translucent</p> <p><i>Rheology:</i> shear thinning with yield stress</p> <p><i>Cost:</i> high</p> <p><i>Stability:</i> unaffected by microorganisms</p>
Cellulose Based	<p><i>Description:</i> water-soluble anionic polymer; examples include 1) sodium carboxymethylcellulose (CMC); 2) hydroxypropylmethylcellulose (HPMC); 3) hydroxyethylcellulose (HEC); 4) hydroxypropylcellulose (HPC)</p> <p><i>Transparency:</i> transparent</p> <p><i>Rheology:</i> slightly thixotropic; shear thinning; no yield stress</p> <p><i>Cost:</i> inexpensive</p> <p><i>Stability:</i> affected by shear, temperature, microorganisms, enzymes, and UV light</p>
Carageenan	<p><i>Description:</i> anionic polysaccharide extracted from red seaweed; three types: iota, kappa, lambda; sodium form is completely water soluble</p>

Table 6.1. Summary of Literature Search Results for Potential Simulants

Material	Characteristics
	<p><i>Transparency:</i> transparent</p> <p><i>Rheology:</i> thixotropic, shear thinning, possesses some yield value</p> <p><i>Cost:</i> inexpensive</p> <p><i>Stability:</i> susceptible to shear and heat degradation</p>
Guar Gum	<p><i>Description:</i> derived from seeds for Guar plant from India/Pakistan region</p> <p><i>Transparency:</i> translucent</p> <p><i>Rheology:</i> shear thinning with no yield stress</p> <p><i>Cost:</i> inexpensive</p> <p><i>Stability:</i> relatively high resistance to shear, temperature, microorganisms, enzymes, UV light</p>
Sodium Alginate	<p><i>Description:</i> water-soluble anionic polysaccharide</p> <p><i>Transparency:</i> translucent</p> <p><i>Rheology:</i> shear thinning with no yield stress</p> <p><i>Cost:</i> high</p> <p><i>Stability:</i> relatively high resistance to microorganisms and enzymes</p>
Gum Arabic	<p><i>Description:</i> naturally occurring gum exuded from stems and branches of the acacia tree</p> <p><i>Transparency:</i> transparent</p>

Table 6.1. Summary of Literature Search Results for Potential Simulants

Material	Characteristics
	<p><i>Rheology:</i> Newtonian below 40 wt%, shear thinning above; exhibits yield value at higher concentrations</p> <p><i>Cost:</i> Relatively expensive due to high concentration required</p> <p><i>Stability:</i> Affected by temperature, microorganisms, enzymes and UV light</p>
<p>Hormite Clay</p>	<p><i>Description:</i> water-dispersible, needle-like particles that form mechanical networks commonly known as attapulgite and sepiolite</p> <p><i>Transparency:</i> opaque</p> <p><i>Rheology:</i> shear thinning with yield stress</p> <p><i>Cost:</i> inexpensive</p> <p><i>Stability:</i> unaffected by temperature, microorganisms, enzymes, UV light; shear sensitive</p>
<p>Other Mineral Suspensions</p>	<p><i>Description:</i> silica/water, talc/water, etc.</p> <p><i>Transparency:</i> translucent or opaque</p> <p><i>Rheology:</i> rheological characteristics vary</p> <p><i>Cost:</i> varies</p> <p><i>Stability:</i> varies</p>

6.1 Transparent Simulant Evaluation

The transparent or translucent simulants shown in Table 6.2 were evaluated against the criteria discussed above. The simulants were scored on a scale of 1–3, where 1 is poor, 2 is fair, and 3 is good. Weighting factors were applied to the criteria such that significant weight was placed on factors that directly affected test success. The scores from each category were multiplied by the weighting factors and summed. These values were normalized to the high score value of 3. Limited information on shear strength was found during the literature search. In general, simulants that develop yield stress also developed shear strength. Therefore, the yield stress information found during the literature search was used to score the shear strength category. Total scores close to 100% represented a good simulant, while those scoring close to 33% were rated poor. Results from this evaluation are shown in Table 6.2.

Laponite, xanthan gum, and carbomers were the top three simulants, with scores greater than 90%. Carbomers were often used as model fluids for yield stress-based experiments (Solomon et al. 1981). Xanthan gum was also recommended by a DuPont consultant as a potential transparent simulant. Laponite has been used in steady jet mixing cavern experiments for the WTP (Enderlin et al. 2003). All three simulants appeared to be good options for further testing.

Table 6.2. Scoring Table of Potential Transparent Simulants

Rank	Utility Functions	Shear Strength	Transparency	Thixotropy	Ease of Prep/Disposal	Expense	Stability	Score
	Weighting factors	0.25	0.25	0.10	0.10	0.10	0.20	
1	Laponite	3	3	1	3	3	3	93%
2	Xanthan Gum	3	3	3	2	3	2	90%
3	Carbomers	3	3	3	2	3	2	90%
4	Polyacrylates	2	3	3	2	2	2	78%
5	Tragacanth Gum	3	2	3	2	1	1	68%
7	Cellulose Based	1	3	3	2	3	1	67%
8	Carageenan	3	2	1	1	2	1	62%
9	Guar Gum	1	2	3	2	2	2	62%
11	Sodium Alginate	1	2	2	2	1	2	55%
12	Gum Arabic	2	1	2	1	1	1	45%
Target Values								
1	Poor							
2	Fair							
3	Good							

6.2 Transparent Simulant Development

In this section, recipes for the transparent simulants, Laponite, Carbopol, and xanthan gum, are presented. Selecting a single transparent simulant for developing the PJM scaling law involved testing the three simulants in a small-scale, single-tube PJM system. Results and experiences with each of the three simulants were used to select the final transparent simulant.

6.2.1 Laponite Recipe

Laponite is a synthetic smectite clay mineral resembling the natural mineral hectorite. Its chemical formula, $\text{Na}(\text{Mg},\text{Li})_3\text{Si}_4\text{O}_{10.5}(\text{OH})_2$, is close to that of hectorite, $\text{Na}_{0.3}(\text{Mg},\text{Li})_3\text{Si}_4\text{O}_{10}(\text{F},\text{OH})_2$, but it has a higher sodium content. Laponite is produced by heat processing of a proprietary gel. Crystallizing the gel produces nanoscale crystals in the form of platelets that are approximately 1 nm thick and 25 nm across (Figure 6.1). When dispersed in water, Laponite forms transparent slurries. The transparency is a result of the small (colloidal) particle size. The slurries are thixotropic. They flow when subjected to shear stress and are stable gels at rest. At rest, the positively charged edges of Laponite particles tend to associate themselves with the negatively charged faces, building stable, voluminous aggregates. Under shear stress, the particles are forced to orient themselves perpendicular to the velocity gradient, decreasing their resistance to flow. At rest, electrostatic forces recover the original gel structure. The rheology of Laponite suspensions can be modified by adding ionic salts or organic polymers. For example, adding organic polymers can change the Laponite slurry from a thixotropic to a rheopectic fluid, turning it to gel under shearing.

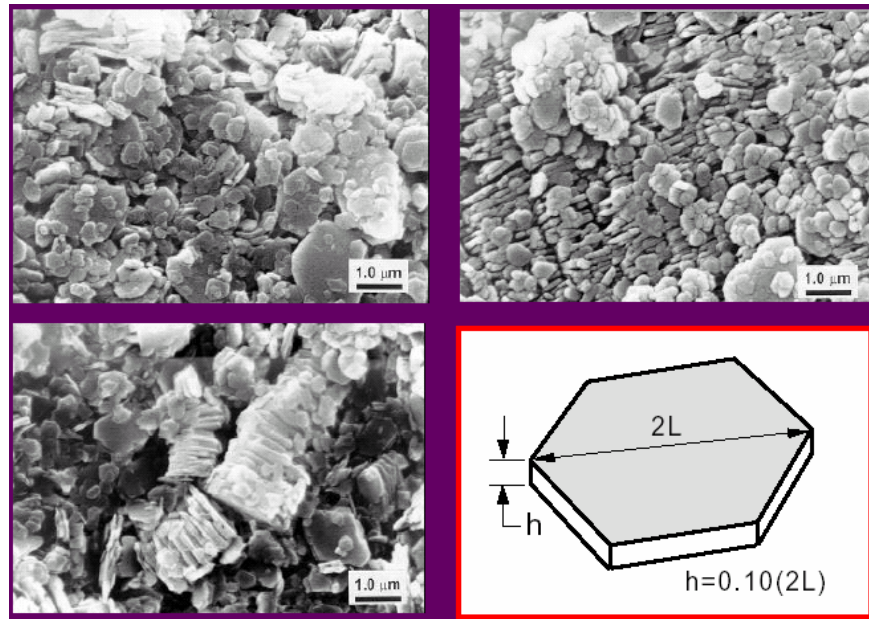


Figure 6.1. Micrographs of Laponite Particles

Because it is highly transparent and easily dispersible in cold water, Laponite RD (Southern Clay Products) was chosen for further testing. As shown in Table 6.2, shear strength is the primary design parameter for PJM testing with a transparent simulant. Preliminary rheological testing was done with Laponite to determine the recipe needed to produce shear strength values in the range of 10–100 Pa. Hanford process water was used for this test. The Laponite gel appeared to reach a steady-state shear strength in approximately 16 to 24 hours. A plot of shear strength versus concentration for Laponite with a gel time of 16 to 24 hours at ambient temperature is shown in Figure 6.2, from which more precise targets could be interpolated. The Laponite recipe chosen for PJM testing based on these data was 1.92 wt% for a target shear strength of approximately 30 Pa.

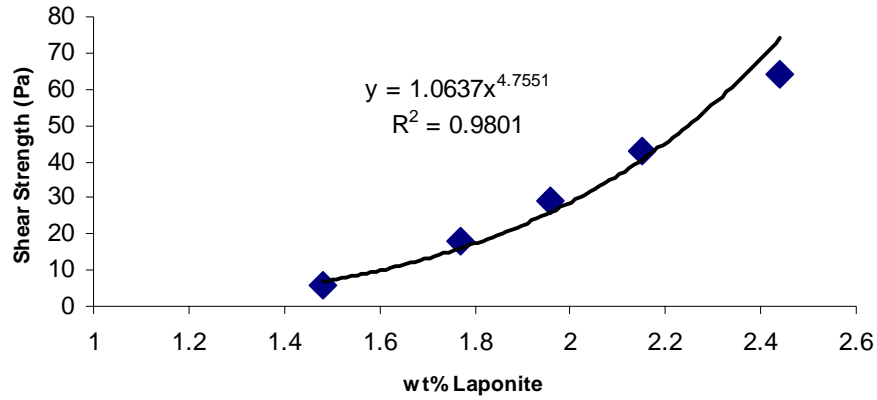


Figure 6.2. Laponite RD Shear Strength as a Function of Concentration in Hanford Process Water at Ambient Temperature with a Gel Time of 16–24 hours

Because many of the PJM test vessels were placed in areas where there was no temperature control, the ambient temperature varied during testing. Because the shear strength samples were placed in relatively small containers next to the PJM test vessels, the temperature of the samples was more readily affected by ambient temperature variations than the contents of large PJM test vessels. Based on data from Speers et al. (1987) on drilling fluids, the potential variation of shear strength due to small temperature differences was expected to be small. Nonetheless, a sample of Laponite was taken and homogenized, then placed in a water bath at controlled temperature. At various gel times (0 to 50 hours after homogenization), a sample was taken and analyzed for shear strength. This procedure was repeated at three temperatures, 15°, 25°, and 35°C. Results from these runs are shown in Figure 6.3. Based on previous experience with shear strength measurements, an error of ±10% was used for the error bars. When these data were fit to Eq. (3.16), the results indicated that the material did approach steady-state shear strength values by the 16–24 hour gel time with minimal impact due to temperature differences between 15° and 35°C, which exceeded the maximum expected temperature variation during testing.

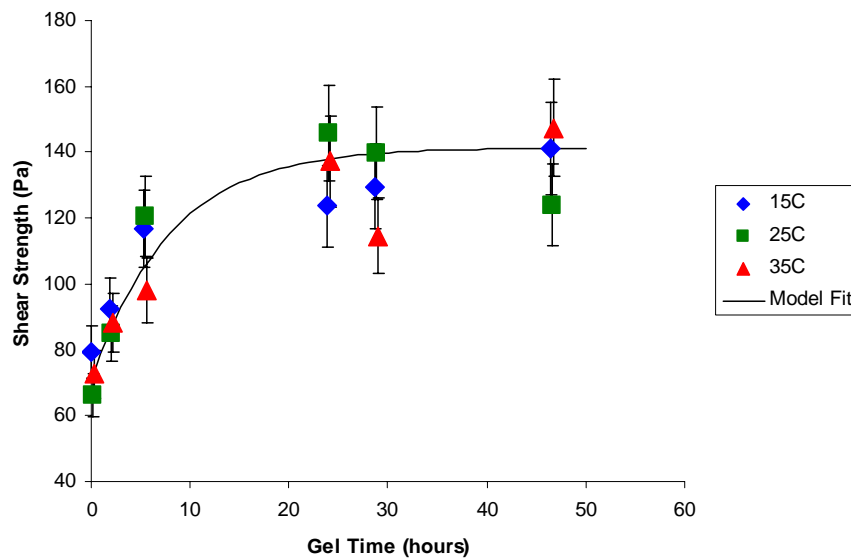


Figure 6.3. Laponite Shear Strength as a Function of Temperature and Gel Time

6.2.2 Carbopol Recipe

Carbopol is a cross-linked acrylic acid polymer (Figure 6.4); Carbopol solution is a translucent to transparent suspension of hydrated spheres of the polymer. Rheologically, a typical Carbopol solution is a pseudoplastic gel whose viscosity increases with concentration and depends strongly on pH. Several Carbopol polymers are available on the market, and their rheological behavior varies widely. Additions of inorganic salts typically decrease the viscosity of a Carbopol solution. The viscosity changes in response to pH, inorganic salts, and shear stress are caused by changes in the morphology of the polymer particles that can be coiled or uncoiled. In a neutral solution, the coiled particles have COOH groups that are associated through hydrogen bonds. An addition of ammonium hydroxide reacts with the acidic groups to form $\text{COO}^-\text{NH}_4^+$ groups, and the particles uncoil into straight chains.

Viscous Carbopol gels form with small concentrations of about 0.1 wt%. Laboratory testing was performed over the range of 0.05 to 0.30 wt% using Hanford process water and Carbopol Ultrez-10 (Noveon, Inc.). This grade of Carbopol goes into solution easily without requiring an organic dispersing agent such as methanol. When dispersed in water, the pH of the solution drops due to the acidic nature of Carbopol; the material must be fully hydrated before the pH is adjusted to neutral. The Carbopol does not thicken until sufficient NaOH is added to raise the pH and expand the polymer spheres. The amount of NaOH required for neutralization usually equals 30 to 40 wt% of the added Carbopol powder.

Carbopol is often used as a model fluid for yield materials but does not possess a true yield stress or shear strength and is often characterized as a shear-thinning fluid. Such fluids are very viscous at low shear rates. As shear rate increases, the viscosity of the fluid often drops several orders of magnitude in a small shear rate range. This behavior produces the effect of a yield material while a true yield stress does not exist. Measurement of shear strength by a shear vane, as shown in Figure 6.5, does not produce the overshoot behavior shown in Figure 3.5. Therefore, the rheogram yield stress must be used to calculate the yield Reynolds number for the PJM scaling law.

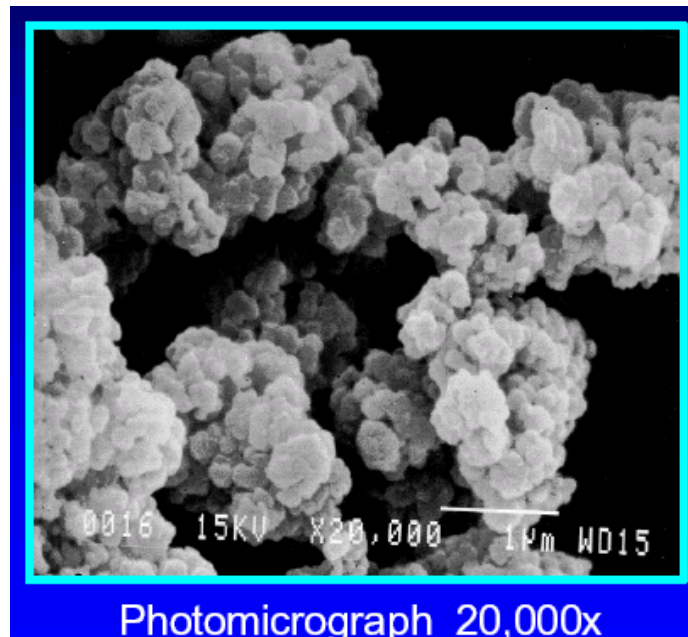


Figure 6.4. Micrographs of Carbopol Particles

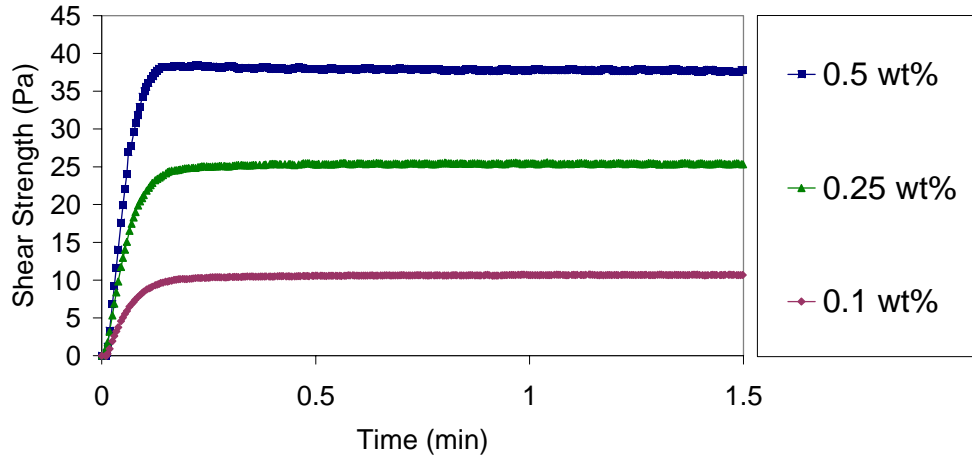


Figure 6.5. Shear Strength Response of Carbopol Ultraez-10 at Various Concentrations and Ambient Temperature

The manufacturer of Carbopol Ultraez-10 recommends using the Casson model (Eq. 3.9) to approximate a yield stress value from a rheogram. Our discussion in Section 3.2 fit rheological data to the Bingham model. From a recipe of Carbopol Ultraez-10 in Hanford process water neutralized with NaOH in a mass ratio of 0.422 NaOH:Carbopol, several concentrations of Carbopol suspensions were prepared. Flow curves were measured at ambient temperature, and Bingham model fit parameters were obtained with correlation coefficients exceeding 0.99. A correlation between the Bingham yield stress and Bingham consistency value as a function of Carbopol concentration is shown in Figures 6.6 and 6.7, respectively. With a target Bingham yield stress of 30 Pa, a formulation of 0.134 wt% Carbopol was used for testing. However, yield Reynolds number calculations were performed using the Casson model fit. Casson yield stress as a function of Carbopol concentration is shown in Figure 6.8. Due to the curvature of the flow, the Casson yield stress values are significantly less than the Bingham yield stresses.

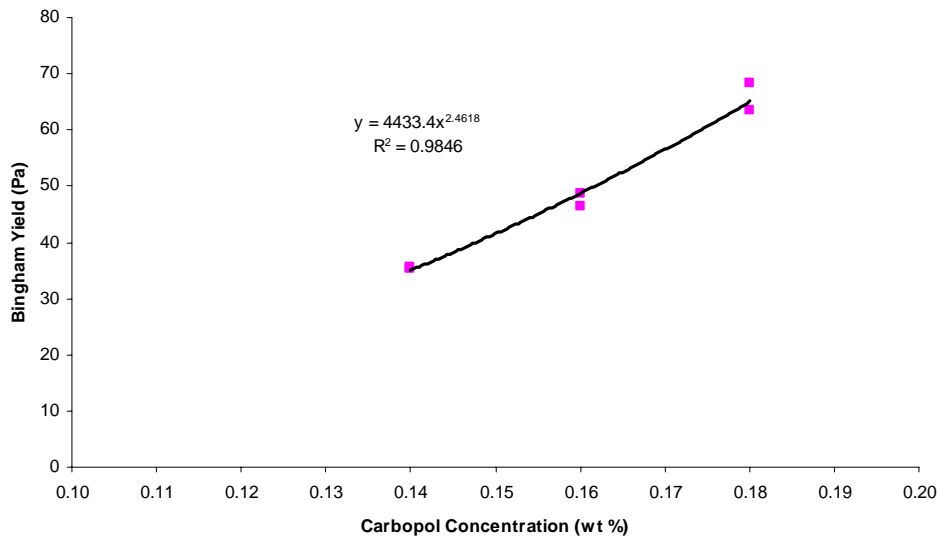


Figure 6.6. Correlation Between Bingham Yield Stress and Carbopol Concentration at Ambient Temperature

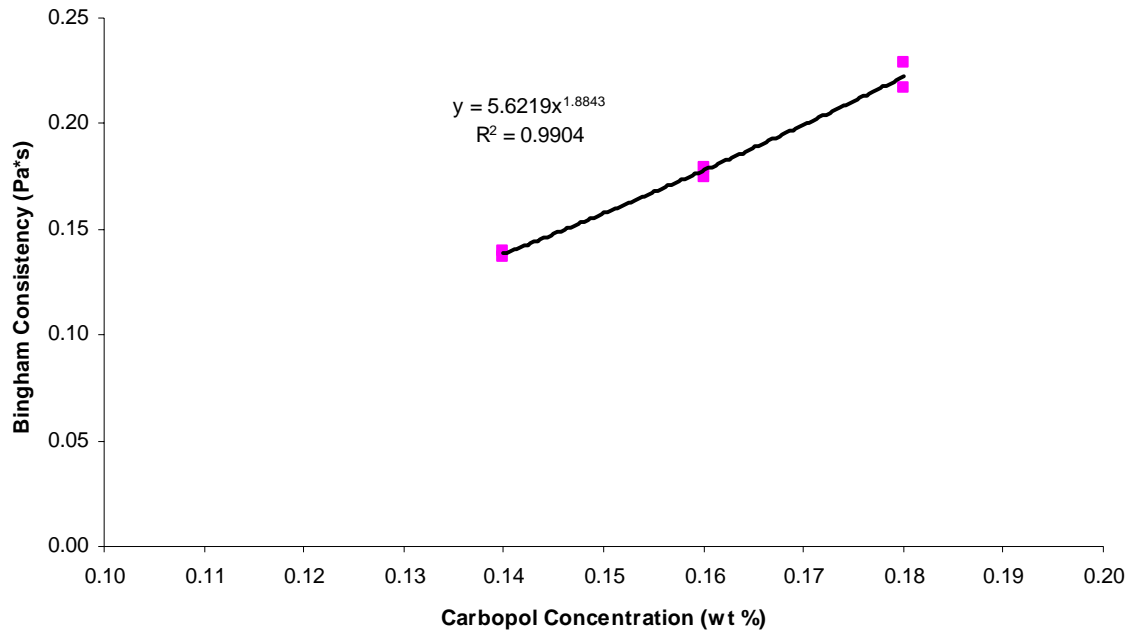


Figure 6.7. Correlation Between Bingham Consistency and Carbopol Concentration at Ambient Temperature

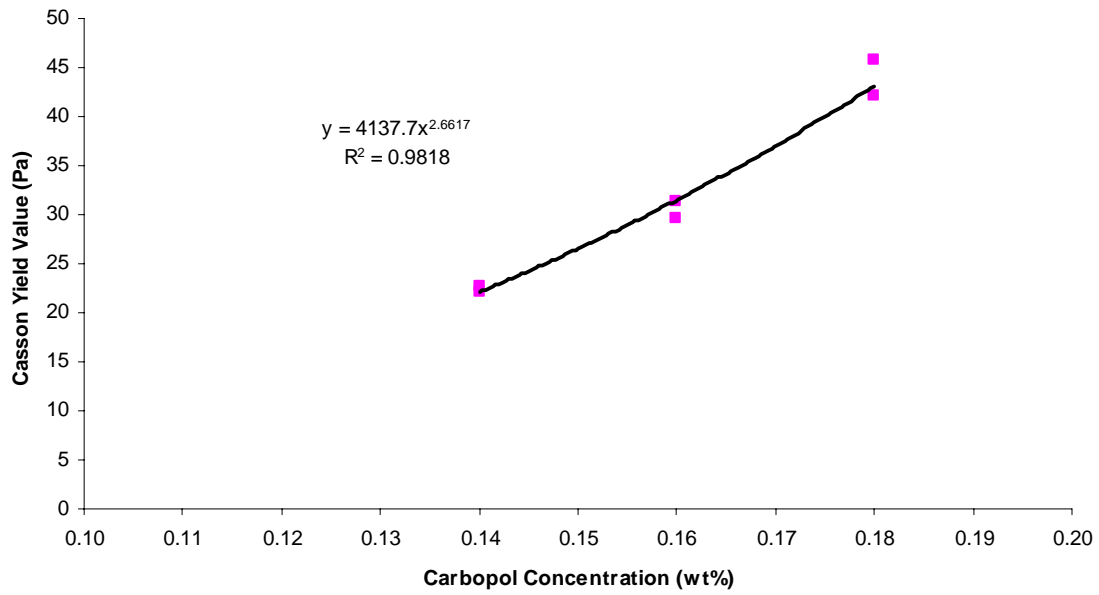


Figure 6.8. Correlation Between Casson Yield Stress and Carbopol Concentration at Ambient Temperature

6.2.3 Xanthan Gum Recipe

Xanthan gum is a microbial polymer, a polysaccharide, produced by bacteria (*Xanthomonas campestris*) to protect their colonies on cabbage or rutabaga leaves. Because of its excellent properties (remarkable resistance to extremes in temperature, pH, and salt concentration), xanthan gum is prepared commercially by aerobic submerged fermentation. The cellulosic molecule of xanthan consists of ~7000 glucose units, as shown in Figure 6.9. The cellulose backbone has trisaccharide side chains with carboxylate groups that carry a negative charge when deprotonated. These mutually repulsive side chains force the cellulosic backbone to adopt a random coil configuration at low ionic strength or high temperature. At low temperature or high ionic strength, the backbone straightens into a helical rod. Addition of electrolyte reduces the negative charge of the side chains. The neutral chains create hydrogen bonds with the backbone protecting it against the influence of changing temperature, pH, and salt concentration. Hydrogen bonding also arranges helical rods into double helix pairs. The loose ends of these pairs become entangled, forming a gel-like consistency. It is so robust that its rheological properties are little affected by pH ranging from 2 to 12, by inorganic salts up to 0.15 M, and by temperature; the solution viscosity drops by a mere several percent as temperature rises from 20° to 80°C.

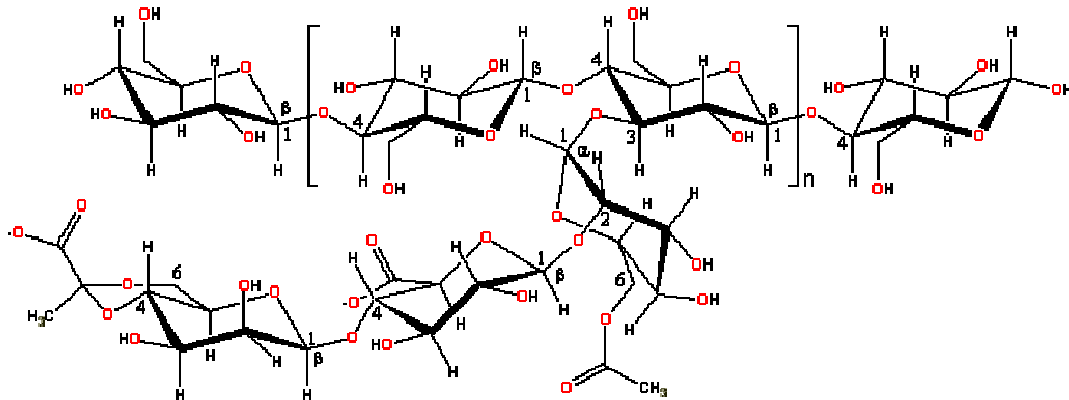


Figure 6.9. Chemical Structure of Xanthan Gum

Rhodicare T (Rhodia, Inc.) was selected as a satisfactory grade of xanthan gum from the manufacturers' claim of high transparency and development of shear strength. A series of Rhodicare T solutions was prepared with Hanford process water at various xanthan gum concentrations between 0.5 and 2.5 wt%. After approximately 24 hours of gel time, shear strengths and rheograms were measured at ambient temperature. The resulting shear strength correlation is shown in Figure 6.10. Rheograms were measured on these samples at ambient temperature, and correlations between Bingham yield stress and Bingham consistency were developed (Figures 6.11 and 6.12, respectively). With a target shear strength of 30 Pa, a target concentration of 2.08 wt% was interpolated from the shear strength correlation. Interestingly, at this value the Bingham yield stress and consistency are close to the bounding pretreated HLW sludge Bingham plastic parameters of 30 Pa for yield stress and 30 cP for consistency.

The xanthan gum solutions were difficult to prepare. Without high-shear mixing, severe lumping or "fish-eyes" were observed. This lumping is due to the hydrophilic nature of xanthan gum. The outer portion of a clump of powder becomes hydrated and keeps the rest of the clump from being wetted. Dissolution of these lumps and air entrainment can be overcome using industrial powder dispersion

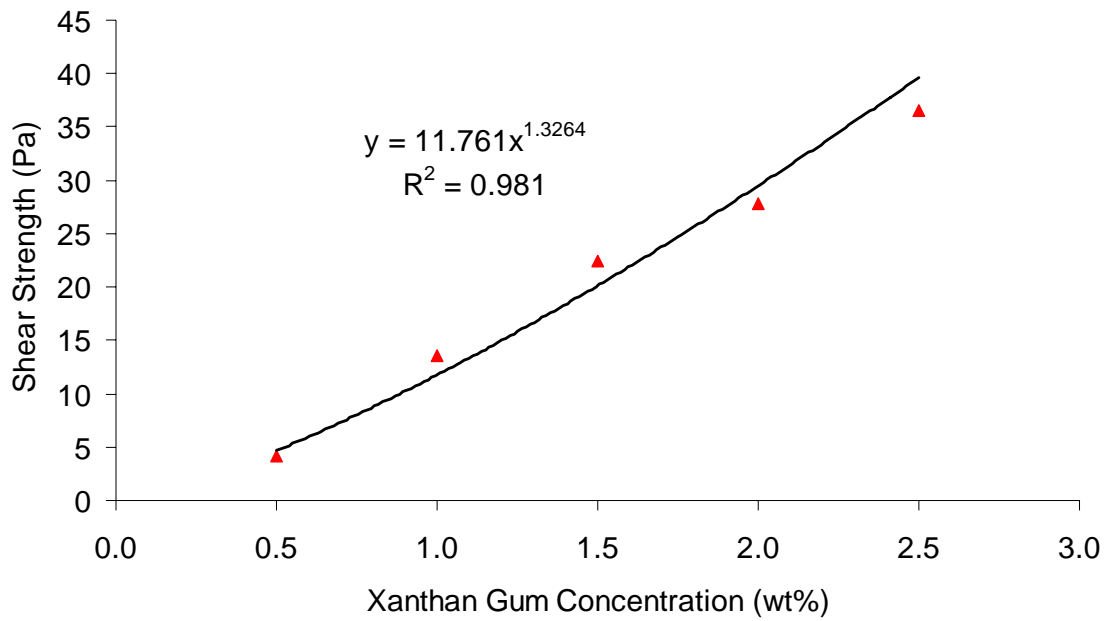


Figure 6.10. Correlation Between Shear Strength and Xanthan Gum Concentration at Ambient Temperature and 24 hour Gel Time

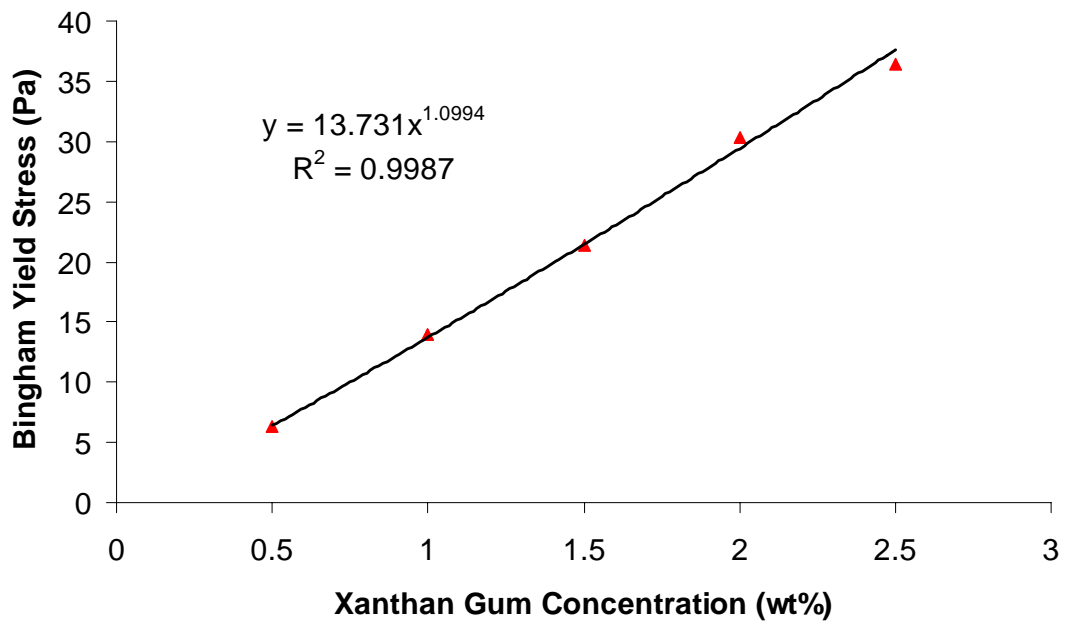


Figure 6.11. Correlation Between Bingham Yield Stress and Xanthan Gum Concentration at Ambient Temperature

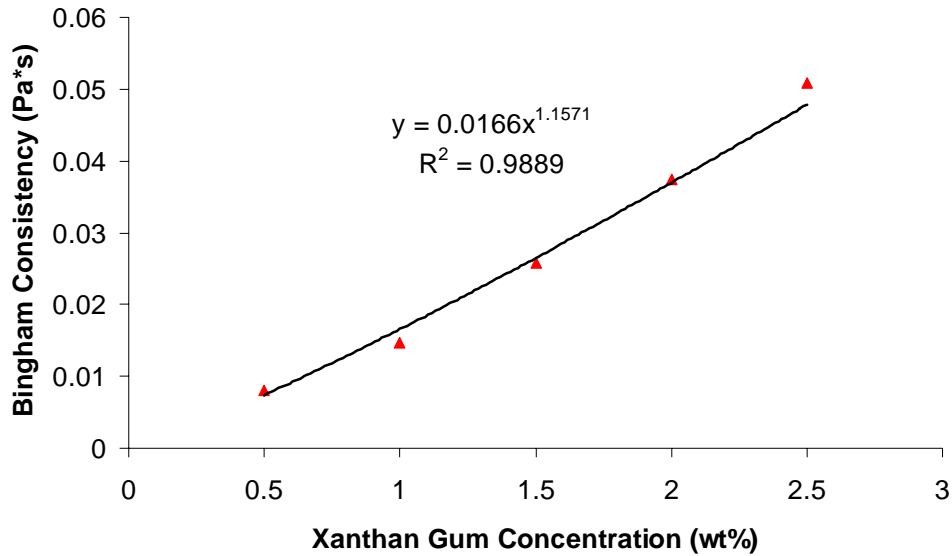


Figure 6.12. Correlation Between Bingham Consistency and Xanthan Gum Concentration at Ambient Temperature

equipment. This equipment may produce transparent solutions at high concentrations but was not readily available for PJM testing. Vendor suggestions for achieving dispersion without specialized equipment included using solvents. This idea was eventually discarded because of the potential impacts to safety (flammability) and waste disposal (organic solvents).

6.2.4 Transparent Simulant PJM Testing

To ensure that the shear strength did not change significantly during testing and to achieve similarity of starting conditions, the Laponite was allowed to age approximately 16 to 24 hours in the PJM testing vessels. Shear strength was determined before testing began. The protocol for gathering shear strength samples for testing was to take the samples immediately after the PJM test stand had been loaded with material and homogenized. These samples were then stored near the test stand so they would age under the same conditions and for the same amount of time as the material in the test stand. At defined points during the testing, including the start and the finish, these undisturbed samples were tested for shear strength. Samples were also pulled from the turbulent cavern via a drain valve on the bottom of the tank near the PJM nozzles, and rheograms were run immediately to determine the rheological properties of the sheared testing material at critical points during the tests.

6.2.4.1 PJM Testing with Laponite

Laponite testing resulted in well-defined cavern formation. Four caverns were measured and their sizes related directly to the operational parameters of the PJM. The optical properties were sufficient for testing and augmented with a tracer dye. Cavern structure was highly visible and thus well documented. However, part of what gives Laponite its gel structure is the charged platelets arranged in sheets. This arrangement caused the Laponite structure to fail in chunks along planes, not slowly eroded by the cavern, leading to caverns forming in discrete steps that may be asymmetric and not completely reproducible.

At the beginning of the PJM test, the shear strength was 29.2 ± 1.9 Pa; at the end it was 31.4 ± 0.5 Pa. Samples were taken from the caverns during PJM mixing and tested in the rheometer. The material in the turbulent cavern region was nearly Newtonian with a viscosity of ~ 10 cP. As expected, the material behaved in a highly thixotropic manner, meaning that the rheology of the material inside the cavern changed as the structure of the gel broke down. This effect was reversible, and the structure rebuilt with time. However, once the gel was broken down and sheared, the cavern maintained nearly constant rheological parameters. The rheology of the Laponite dropped relatively slightly during the several-hour test from the first cavern measurement to the fourth (Figure 6.13).

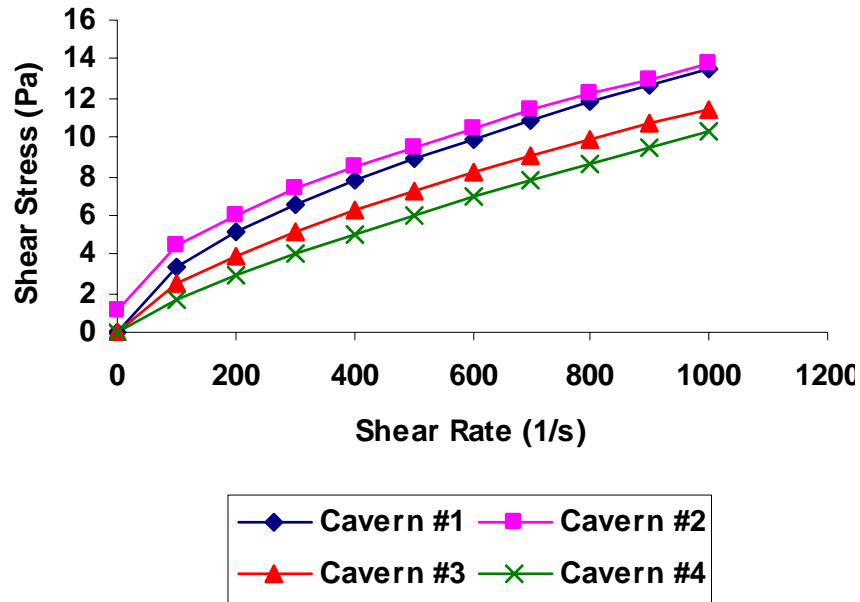


Figure 6.13. Flow Curves of Laponite Samples Drawn from PJM Mixing Caverns at Ambient Temperature

6.2.4.2 PJM Testing with Carbopol

The Carbopol caverns were more difficult to define with precision, but measurable caverns were formed. After the Carbopol was prepared at 0.134 wt%, samples were taken from the mixing cavern during the PJM test. The Casson model was used for calculating yield stress for the yield Reynolds number. The starting Casson yield stress of the material was ~ 19 Pa, the ending value ~ 13 Pa. For comparison, in the other materials the highest Bingham model parameters measured during testing were 33 Pa for yield stress and 100 cP for consistency. As discussed in Section 6.2.2, Carbopol does not exhibit true shear strength, and shear vane tests were not performed.

As shown in Figure 6.14, the rheological properties of the Carbopol cavern samples dropped during the course of testing due to shear degradation in the pulse tube and its effects on the Carbopol structure. The PJM testing put extensive stresses on the material for several hours. This structure degradation effect was irreversible. Therefore, while the Carbopol is not thixotropic it is shear sensitive, and the rheological yield values decrease as high shear rates are applied over long periods of time.

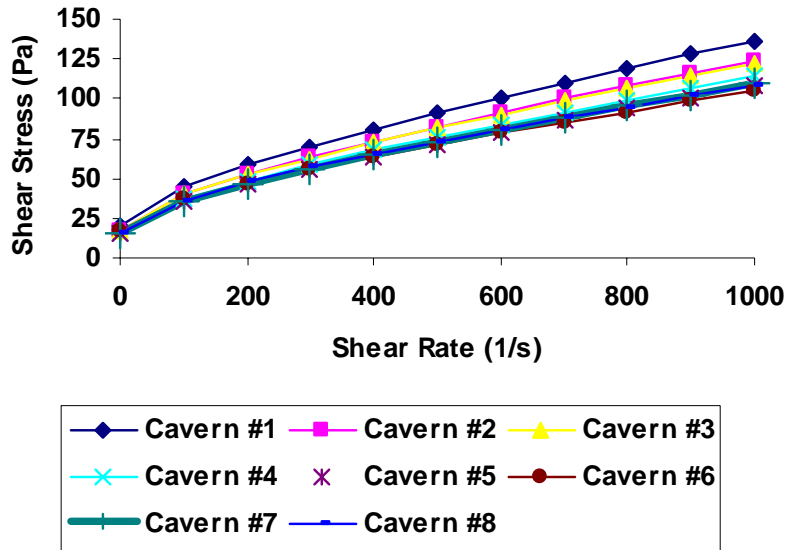


Figure 6.14. Flow Curves of Carbopol Samples Drawn from PJM Mixing Caverns at Ambient Temperature

6.2.4.3 PJM Testing with Xanthan Gum

Three cavern height measurements were performed using this simulant. The shear strength at the start of the test was 36.3 ± 1.3 Pa, and 38.4 ± 2.5 Pa at the end. Samples were taken from the mixing cavern at each steady-state cavern. Examination showed that the yield point remained unchanged during the course of testing (Figure 6.15). The average rheology measured during testing, fit with a Bingham model, was approximately 35 Pa for yield stress and 40 cP for consistency. Additionally, the xanthan gum was observed to be easily infected by bacterial growth. This limited the useful life of the solution to several days rather than the several weeks desired by the PJM testing program.

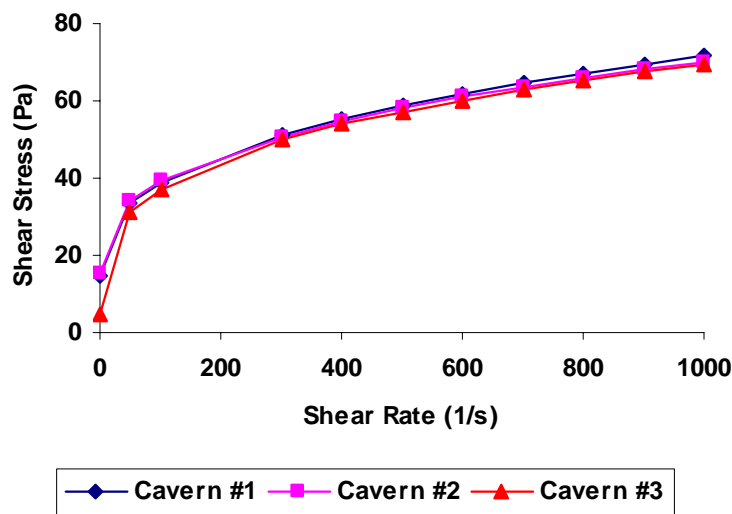


Figure 6.15. Flow Curves of Xanthan Gum Samples Drawn from PJM Mixing Caverns at Ambient Temperature

6.2.5 Transparent Simulant PJM Testing Downselect

Important mixing parameters were explored with every simulant, and each one displayed unique mixing properties and presented different complexities for modeling the resultant behavior. The Laponite was thixotropic and not viscous enough to be ideal with regard to the viscous Reynolds number. The Carbopol was not thixotropic but does not have real shear strength. However, the Carbopol degrades irreversibly over the course of prolonged testing due to exposure to high shear. The xanthan gum modeled the target rheology most accurately based on rheograms, but the bacterial growth in the Rhodicare meant the material could not be reused and presented a disposal issue.

Rheologically, each simulant met the goal properties of approximately 30 Pa for shear strength (Table 6.3). Based on the discussion in Section 4, these values were used to calculate yield Reynolds numbers for each PJM operating condition. The yield Reynolds number is the primary factor in determining a PJM scaling law. Because Carbopol does not have shear strength, the Casson yield stress was used for this calculation.

Bingham Reynolds number was also a factor in determining the PJM scaling law. The Bingham parameters for each of the simulants are shown in Table 6.3, while a comparison to the HLW pretreated sludge upper bounding target (see Section 3.2) of 30 Pa Bingham yield stress and 30 cP Bingham consistency is shown in Figure 6.16. It is apparent that the Laponite was not viscous enough for a good flow curve match to the WTP upper bound; the xanthan gum is a relatively good fit, while the Carbopol is much too viscous.

Table 6.3. Significant Opaque Simulant Properties for PJM Performance and Goal Values

Description	Concentration (wt%)	Bingham Consistency (cP)	Bingham Yield Stress (Pa)	Shear Strength (Pa)
Laponite	1.92	10	0	30
Carbopol	0.134	100	33	13–19 (Casson model yield)
Xanthan Gum	2.08	40	35	37

When the relevant PJM operating parameters were compiled and the nondimensional cavern height and yield Reynolds number calculated, the plotted variables should follow the relationship described by Eq. (4.13). Because the tests were performed in the same PJM vessel, the constants in Eq. (4.13) were identical for various simulants. This suggests that if all of the significant properties were captured by Eq. (4.13), the data would follow the same nondimensional correlation regardless of simulant. PJM scaling results from several sets of simulant tests are shown in Figure 6.17. In addition to the simulant tests described above, additional Laponite, Carbopol, and xanthan gum solutions were prepared with different rheological goals. PJM tests were performed on these simulants; results are shown in the figure.

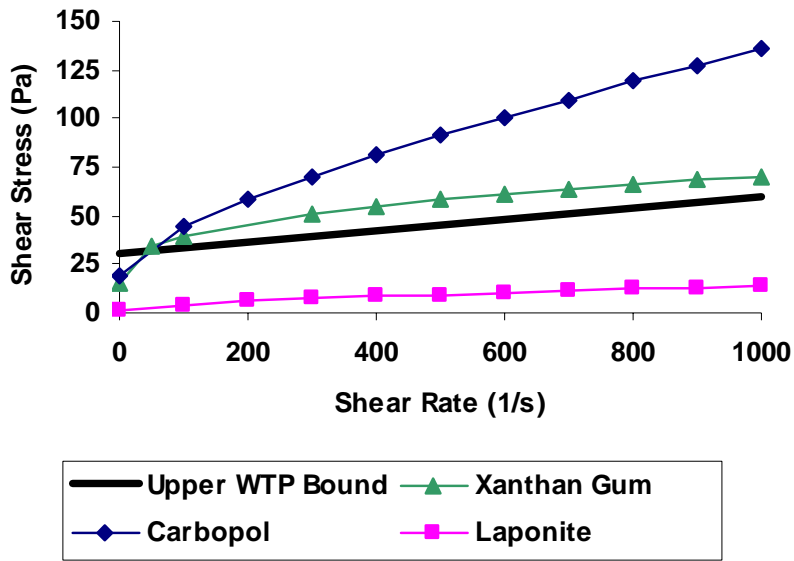


Figure 6.16. Comparison of Transparent Simulant Flow Curves to the WTP HLW Pretreated Sludge Upper Rheological Bound at Ambient Temperature

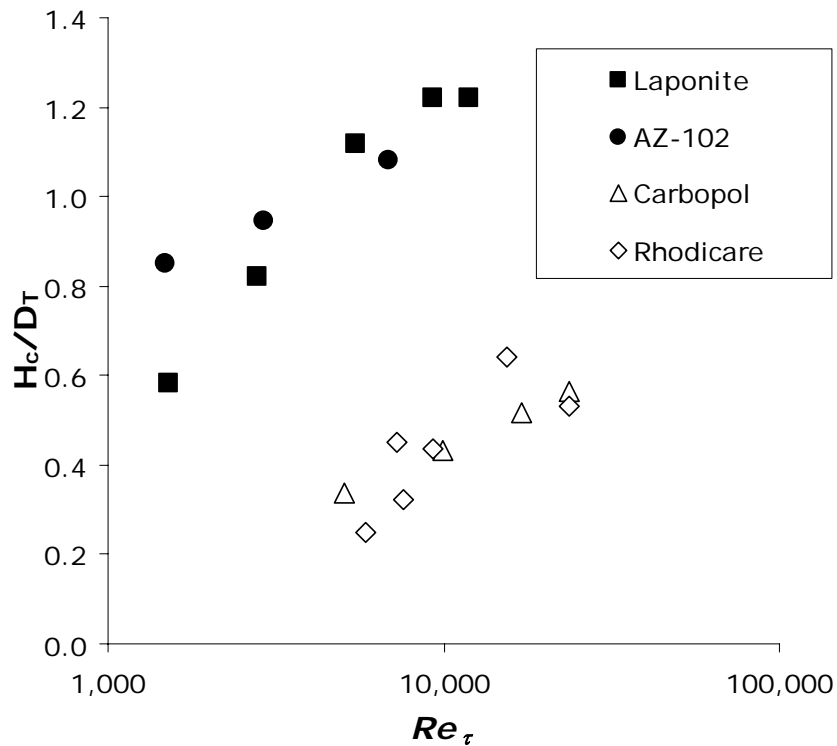


Figure 6.17. Nondimensional PJM Scaling Correlation for Several Simulants and Operating Conditions

Contrary to expectations that a single correlation would be observed in Figure 6.17, two non-dimensional correlations were observed, one for Laponite and another for Carbopol and xanthan gum. From these correlations, one can see that the performance (i.e., cavern height) of the Laponite simulant far exceeds that of Carbopol and xanthan gum. Because the Bingham Reynolds number is expected to affect the correlation only moderately, flow curve differences should not produce this degree of performance change. Therefore, another unaccounted parameter is the likely source of this difference.

The difference is hypothesized to be the viscoelasticity of the simulants. Polymer-based materials are known to have significant viscoelastic properties (see Table 3.6) because the polymer chain compresses and stretches with shear rather than moving with the bulk fluid. Conversely, particulate slurries may rearrange in packing structure, but individual particles do not significantly compress and stretch as in polymer-based systems. Therefore, particulate slurries typically possess significantly lower levels of viscoelasticity than polymer-based systems.

When a viscoelastic fluid is forced through the PJM nozzle, a high level of shear is placed on the fluid in a relatively short period of time. For instance, the shear rate through a 1-inch-diameter nozzle at a velocity of 10 ft/sec is approximated by the velocity over the radius of the tube, or 240 s^{-1} . Using these parameters, Eq. (3.15) can be used to calculate the relaxation time for the xanthan gum and Carbopol solutions described in Table 3.5. The process time is defined as the time when the fluid discharges from the nozzle to another location in the tank and can be calculated from Eq. (4.14). Using a jet decay coefficient of 1 and noting that water has a relaxation time of 10^{-12} while the viscoelastic silicone polymer “silly putty” has a relaxation time of 0.3 (Steffe 1996), the plot shown in Figure 6.18 was created. This plot illustrates that fluids such as silly putty, Carbopol, and xanthan gum are expected to behave as viscoelastic fluids near the end of the nozzle. As flow proceeds, the Deborah number is reduced and the fluids flow in a viscous manner. Viscoelastic rather than fully viscous flow near the end of the nozzle would dissipate mixing energy faster and result in smaller caverns. This effect is expected to be amplified in the case of non-steady jet systems, when the viscous flow regions far from the nozzle cannot be fully established due to drive time limitations.

To verify that the performance of the PJM systems with actual pretreated HLW sludge is similar to the Laponite correlation or the Carbopol and xanthan gum correlation, additional PJM tests were performed with an AZ-102 pretreated sludge simulant provided by BNI. Because this simulant is opaque, a tracer dye was added to the mixing cavern, and dyed regions on the PJM vessel walls were used to estimate cavern height. Results from these tests are shown in Figure 6.17. These data follow the Laponite correlation. On this basis, Laponite was selected as the transparent PJM simulant for determining a PJM scaling law.

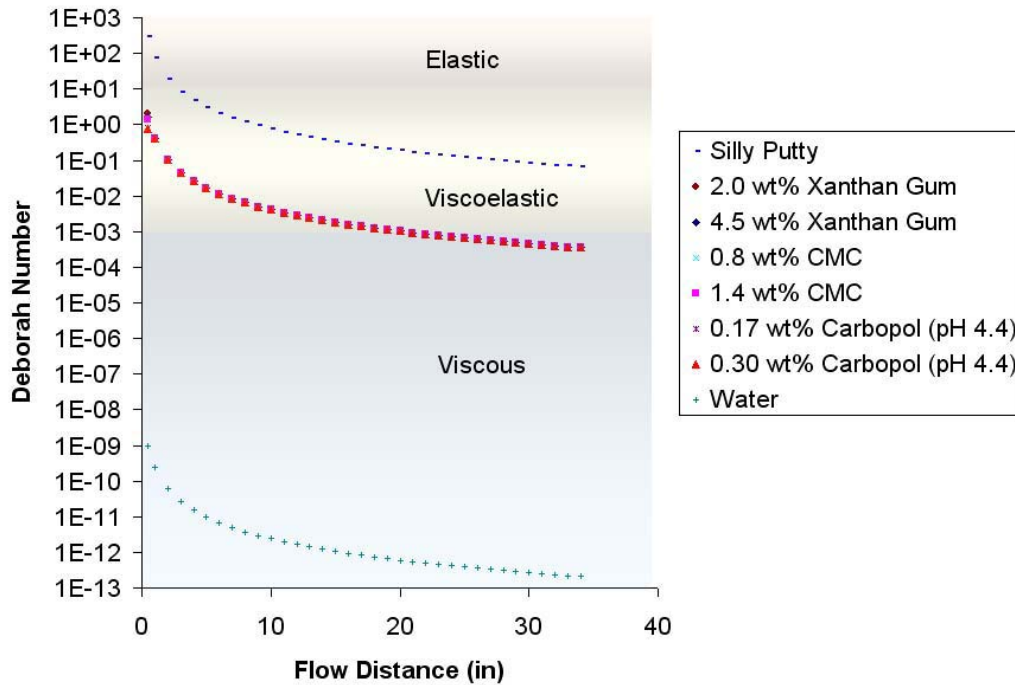


Figure 6.18. Deborah Number as a Function of Flow Distance in a PJM Vessel (nozzle velocity is 10 ft/sec through a 1-in.-diameter nozzle with a jet decay coefficient of 1)

6.3 Opaque Simulant Evaluation

Similar to the transparent simulants, the opaque simulants shown in Table 6.1 were evaluated against the criteria discussed early in Section 6. The simulants were scored by a scale of 1–3 where 1 is poor, 2 is fair, and 3 is good. Significant weight was placed on factors that directly affected test success. The scores from each category were multiplied by the weighting factors and summed. These values were normalized to the high score value of 3. Total scores close to 100% represent a good simulant, while those close to 33% represent poor simulants. Results of this evaluation are shown in Table 6.4.

Table 6.4. Scoring Table of Potential Opaque Simulants

Rank	Utility Functions	Yield Stress	Consistency	Thixotropy	Ease of Prep/Disposal	Expense	Stability	Score (%)
	Weighting Factors	0.25	0.15	0.15	0.10	0.10	0.25	
1	Kaolin-Bentonite Clay	3	3	2	3	3	3	95
2	Hormite Clay	3	2	2	3	2	2	78
3	Mineral Suspensions	2	2	2	2	1	3	72
4	AZ-102 HLW Pretreated Sludge Simulant	1	1	2	2	1	3	72
1	Poor							
2	Fair							
3	Good							

Kaolin-bentonite clay was the top scorer at over 90%. Hormite clay appeared to be a good option, but its sensitivity to shear led to issues with stability, thixotropy, and expense. Mineral suspensions were an option, but identification of a satisfactory mineral and subsequent recipe would require too long a development time. For these reasons, mineral suspensions scored fair for rheological properties and poor for expense. The AZ-101 HLW pretreated sludge simulant discussed in Section 6.2.5 was also evaluated. With a Bingham yield stress of approximately 5 Pa and a consistency of approximately 10 cP, its rheological properties were lower than the goal Bingham plastic parameters. Because the simulant consists of several rare metallic elements, it costs more than the other options. This simulant is also difficult to prepare and would need to be ordered from a chemical manufacturer with a large lead time. Based on this evaluation, kaolin-bentonite clay was chosen for the scaled prototypic PJM tests.

6.4 Opaque Simulant Development

Clay suspensions are used widely in industry and commonly exhibit a shear-thinning pseudoplastic flow. Brownian motion, van der Waals forces, and electrostatic forces determine the interactions between clay particles. The main mode of particle interaction is flocculation, or formation of agglomerates. The agglomerates organize themselves into a three-dimensional structure or coagulated suspension that resists flow. When shear is placed on the structure it breaks down, and the suspension flows. As shear increases agglomerate size decreases, resulting in diminishing viscosity—characteristic of a pseudoplastic fluid. In this manner, interaction between the agglomerates contributes to energy dissipation during viscous flow.

Fortunately, Rassat et al. (2003) developed a simulant for Hanford tank retrieval studies. This simulant was a mixture of 80% kaolin (EPK Feldspar Pulverized) and 20% bentonite (WYO-Ben Big Horn CH-200) powder mixed to various solids concentrations in Hanford process water. This recipe produced a simulant with Bingham plastic properties near the goal of 30 Pa yield stress and 30 cP consistency. Additionally, the simulant appeared to develop shear strength in range of 10–100 Pa. These properties appeared to occur at a solids loading in the 20–30 wt% range.

Consequently, several laboratory-scale samples were prepared using this recipe at various solids concentrations. Flow curves were measured for each sample and a correlation between Bingham consistency (Figure 6.19) and Bingham yield stress (Figure 6.20) was developed. To achieve the target 30 Pa yield stress, the recipe called for 27 wt% kaolin-bentonite clay. The density of the simulant at 27 wt% is approximately 1.18 g/mL.

Although not the primary design parameter for an opaque simulant, the shear strength behavior of the kaolin-bentonite simulant was investigated in a manner similar to Laponite. Initial shear-strength-versus-gel-time curves are shown in Figure 6.21. These indicate that the shear strength of kaolin-bentonite clay developed over a longer period of time than Laponite.

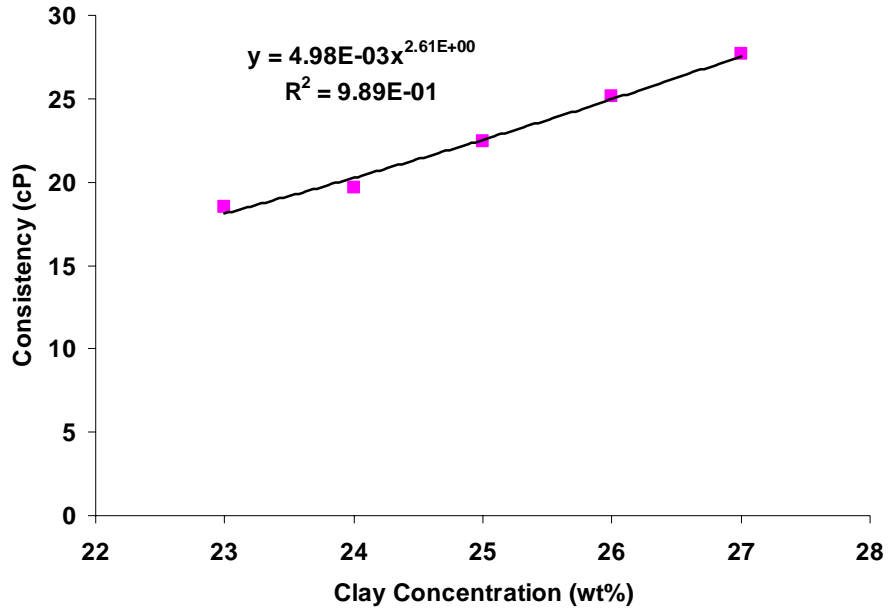


Figure 6.19. Correlation Between Bingham Consistency and Kaolin-Bentonite Concentration at Ambient Temperature

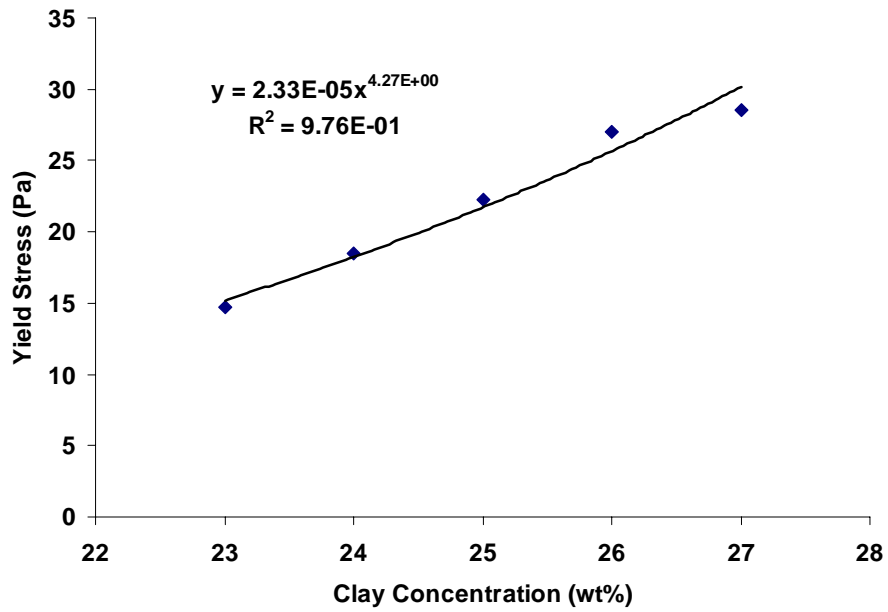


Figure 6.20. Correlation Between Bingham Yield Stress and Kaolin-Bentonite Concentration at Ambient Temperature

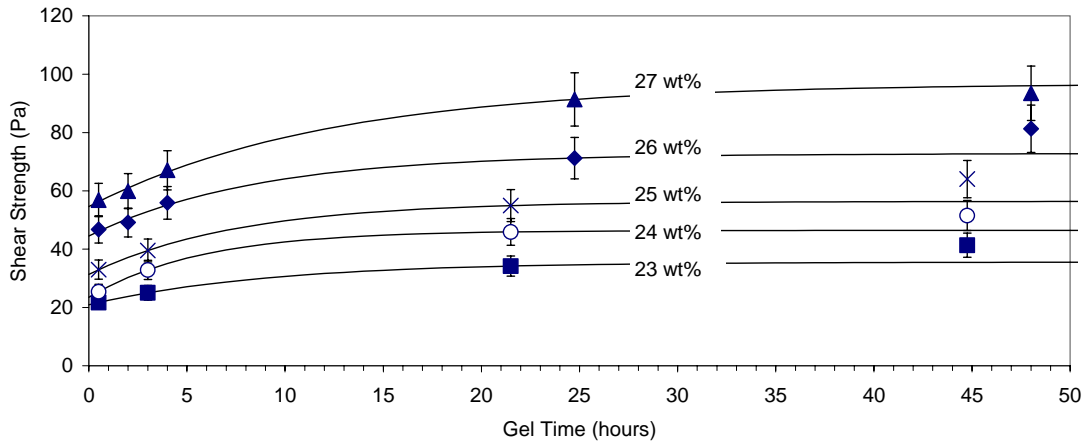


Figure 6.21. Shear Strength as a Function of Gel Time for Kaolin-Bentonite Simulant at Various Solids Concentrations at Ambient Temperature

To investigate the effect of temperature on shear strength, a sample of kaolin-bentonite simulant was taken and homogenized, then placed in a water bath at controlled temperature. At various gel times (0 to 100 hours after homogenization), the sample was analyzed for shear strength. This procedure was repeated at 15°, 25°, and 35°C. Results are shown in Figure 6.22. Based on previous experience with shear strength measurements, an error of $\pm 10\%$ was used for the error bars. When the data were fit to Eq. (3.16), results indicated temperature had a significant effect on shear strength. The shear strength development appeared to increase as temperature increased from 15° to 35°C. If shear strength measurements are required during PJM testing with the kaolin-bentonite samples, steps should be taken so the temperature of the samples used for shear strength is close to the temperature of the bulk vessel.

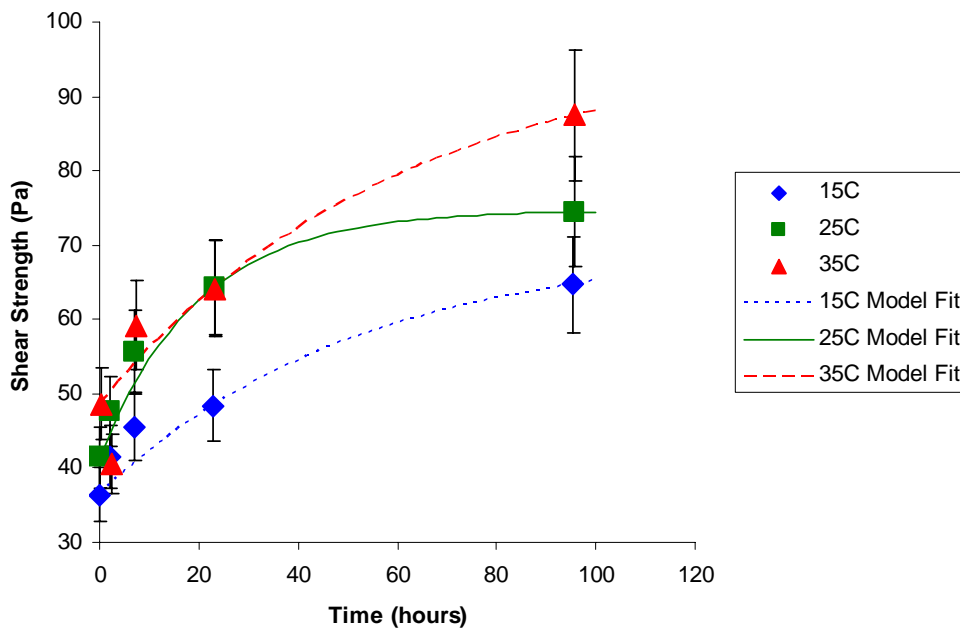


Figure 6.22. Kaolin-Bentonite Shear Strength as a Function of Temperature and Gel Time

7.0 Conclusions

A mathematical prediction of the performance of PJM vessels identified several significant rheological properties. To test this mathematical prediction and support the design of full-scale PJM vessels for the WTP, a two-stage PJM project was implemented. The first stage involved verification of a PJM scaling-law that would allow tests conducted at small scale to be applied to larger-scale systems. This step required a transparent simulant so PJM mixing performance could be observed and measured directly. In this case, only shear strength was considered significant to PJM performance. Three transparent simulants were tested: Laponite RD, Carbopol Ulrez-10, and xanthan gum (Rhodicare T). It was hypothesized that the viscoelastic properties of the Carbopol and xanthan gum significantly limited the effectiveness of the PJM vessel. An additional test with a WTP process simulant was performed to confirm these limitations. Consequently, Laponite was chosen as the simulant to confirm PJM scaling laws. Table 7.1 summarizes the significant rheological properties for PJM performance during transparent simulant testing. Target values and actual Laponite simulant values are shown. This table indicates that Laponite meets the objectives for transparent PJM testing.

Table 7.1. Summary of Significant Transparent Simulant Properties for PJM Performance

Property	Goal Values	Simulant Values
Shear Strength	<ul style="list-style-type: none"> • 30 Pa (normal operation) • 80 Pa (restart condition) 	Adjustable in this range based on Laponite and salt concentrations and aging time. With Hanford process water and 16–24 hour gel time at ambient temperature, the following correlation from Figure 6.2 applies to 1.5 and 2.5 wt% Laponite: $y = 1.06 x^{4.76}$ where y is shear strength (Pa) and x is wt% Laponite, approximately 30 Pa at 1.5 wt% and 80 Pa at 2.5 wt%.

For the second stage of PJM testing, scaled prototypic versions of potential full-scale WTP PJM vessels were tested with an opaque simulant. The opaque simulant was designed to match actual pretreated HLW sludge rheological properties that were identified as significant to PJM performance. The opaque simulant developed was based on a previous Hanford tank retrieval simulant that consisted of a mixture of kaolin clay (EPK Feldspar Pulverized) and bentonite clay (WYO-Ben Big Horn CH-200) in Hanford process water. The recipe calls for a composite of 80% kaolin and 20% bentonite mixed with Hanford water to a loading of approximately 27 wt%. Table 7.2 shows a summary of the significant rheological properties to PJM performance during opaque simulant testing. Goal values and actual kaolin-bentonite simulant values are also shown. This table indicates that kaolin-bentonite simulant meets the objectives for opaque PJM testing.

Table 7.2. Summary of Significant Opaque Simulant Properties for PJM Performance and Goal Values

Property	Goal Values	Simulant Values
Density	1.2 g/mL	1.18 g/mL at 27 wt%
Bingham Consistency	30 cP	Adjustable; with Hanford process water at ambient temperature, the following correlation from Figure 6.19 applies between 23 and 27 wt% kaolin-bentonite: $y = 0.005 x^{2.61}$ where y is the consistency (cP) and x is the wt% kaolin-bentonite clay, approximately 30 cP at 27 wt%.
Bingham Yield Stress	30 Pa	Adjustable; with Hanford process water at ambient temperature, the following correlation from Figure 6.20 applies between 23 and 27 wt% kaolin-bentonite: $y = 2.33 \times 10^{-5} x^{2.61}$ where y is the yield stress (cP) and x is the wt% kaolin-bentonite clay, approximately 30 Pa at 27 wt%

8.0 References

- Alderman NJ, GH Meetenm, and JD Sherwood. 1991. "Vane rheometry of bentonite gels." *J. Non-Newtonian Fluid Mech.* 39:291-310.
- Avramidis KS and RM Turain. 1991. "Yield Stress of Laterite Suspensions." *J. Colloid Interface Sci.* 143:54-68.
- Barnes HA and JO Carnali. 1990. "The vane-in-cup as a novel rheometer geometry for shear-thinning and thixotropic materials." *J. Rheol.* 34(6):841-866.
- Bowles JE. 1977. *Foundation, Analysis and Design*, 2nd Ed. McGraw-Hill, New York.
- Braun DB and W Rosen. 1999. *Rheology Modifiers Handbook*. William Andrew Publishing, Norwich, NY.
- Chhabra RP and JF Richardson. 1999. *Non-Newtonian Flow in the Process Industries*. Butterworth Heinemann, Oxford, England.
- Ciullo PA (ed.). 1996. *Industrial Minerals and Their Uses*. Noyes Publications, Westwood, NJ.
- Davidson RL (ed.). 1980. *Handbook of Water-Soluble Gums and Resins*. McGraw-Hill, NY.
- Dzuy NQ and DV Boger. 1985. "Direct Yield Stress Measurement with the Vane Method." *J. Rheology* 29:335-347.
- Enderlin CW, MG Dodson, F Nigl, J Bontha, and JM Bates. 2003. *Results of Small-Scale Particle Cloud Tests and Non-Newtonian Fluid Cavern Tests*. WTP-RPT-078 Rev. 0, Battelle – Pacific Northwest Division, Richland, WA.
- James AE, DA Williams, and PR Williams. 1987. "Direct measurement of static yield properties of cohesive suspensions." *Rheol. Acta.* 26:437-446.
- Keentok M. 1982. "The measurement of the yield stress of liquids." *Rheol. Acta* 21:325-332.
- Keentok M, JF Milthorpe, and E O'Donovan. 1985. "On the shearing zone around rotating vanes in plastic liquids: theory and experiment." *J. Non-Newtonian Fluid Mech.* 17:23-35.
- Lapasin R and S Pricl. 1995. *Rheology of Industrial Polysaccharides*. Blackie Academic and Professional, London.
- Liddell PV and DV Boger. 1996. "Yield Stress Measurements with the Vane." *J. Non-Newtonian Fluid Mech.* 63:235-261.

McBain GD, JA Harris, YK Leong, and S Vigh. 2000. "Viscoelastic characterization of low-grade molasses by jet-swell measurements." *Proceedings of Australian Society of Sugar Cane Technologists*, DM Hogarth, ed., pp. 467–473.

Nguyen QD and DV Boger. 1983. "Yield Stress Measurement for Concentrated Suspensions." *Rheol. Acta*. 27:321-349.

Nguyen QD and DV Boger. 1985a. "Thixotropic Behavior of Concentrated Bauxite Residue Suspensions." *Rheol. Acta*. 24:427-437.

Nguyen QD and DV Boger. 1985b. "Direct Yield Stress Measurements with the Vane Method." *Rheol. Acta*. 29:335-347.

Poloski AP, PR Bredt, JW Chenault, and RG Swoboda. 2003. *Rheological and Physical Properties of AZ-101 HLW Pretreated Sludge and Melter Feed*. WTP-RPT-096 Rev. 0, Battelle – Pacific Northwest Division, Richland, WA.

Poloski A. 2004. *Technical Basis for HLW Vitrification Stream Physical and Rheological Property Bounding Conditions*. WTP-RPT-100 Rev. 0, Battelle – Pacific Northwest Division, Richland, WA.

Rajaratnam N. 1976. *Turbulent Jets*. Elsevier Scientific Publishing Co., New York.

Rassat SD, LM Bagaasen, LA Mahoney, RL Russell, DD Caldwell, and DP Mendoza. 2003. *Physical and Liquid Chemical Simulant Formulations for Transuranic Wastes in Hanford Single-Shell Tanks*. PNNL-14333, Pacific Northwest National Laboratory, Richland WA.

Smith GL and K Prindiville. 2002. *Guidelines for Performing Chemical, Physical, and Rheological Properties Measurements*. 24590-WTP-GPG-RTD-001 Rev. 0, Bechtel National, Inc., Richland, WA.

Solomon J, TP Elson, and AW Nienow. 1981. "Cavern Sizes in Agitated Fluids with a Yield Stress." *Chem. Eng. Commun.* Vol. 11, pp. 143-164.

Speers RA, KR Holme, MA Tung, and WT Williamson. 1987. "Drilling fluid shear stress overshoot behavior." *Rheologica Acta*, Vol. 26, pp. 447-452.

Steffe JF. 1996. *Rheological Methods in Food Process Engineering*, 2nd Edition. Freeman Press. An online version of this book can be downloaded from <http://www.egr.msu.edu/~steffe/freebook/offer.html>.

Tanner RI. 1988. *Engineering Rheology*, revised ed., Clarendon, Oxford, England.

van Olphen H. 1977. *An Introduction to Clay Colloid Chemistry*. Wiley and Sons, New York.

Distribution

**No. of
Copies**

**No. of
Copies**

OFFSITE

ONSITE

1 Savannah River National Laboratory
Richard Edwards
Westinghouse SA
Aiken, South Carolina 29808-0001

9 Battelle – Pacific Northwest Division
P. R. Hrma K6-24
L. K. Jagoda K6-24
D.E. Kurath P7-28
P. A. Meyer K7-15
A.P. Poloski P7-25
Project Office (2) P7-28
Information Release (2) K1-06

5 Bechtel National, Inc.
H. A. Abodishish H4-02
S. M. Barnes H4-02
G. L. Smith H4-02
J. F. Doyle (2) H4-02